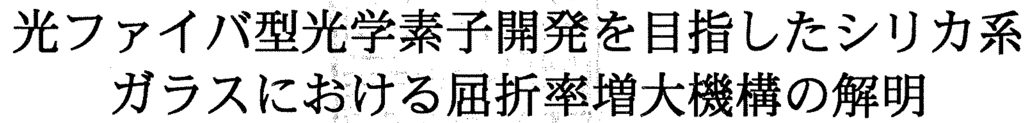

光ファイバ型光学素子開発を目指したシリカ系ガラスにおける屈折率増大機構の解明

課題番号 12450132

平成12年度～14年度科学研究費補助金
[基盤研究(B)(2)]研究成果報告書

平成15年4月

研究代表者　大木義路
(早稲田大学理工学部教授)

はしがき

本報告書は下記の課題で助成を受けた平成12年度～平成14年度科学研究費補助金[基盤研究(B)(2)]に関わる研究成果をまとめたものである。

研究課題

光ファイバ型光学素子開発を目指したシリカ系ガラスにおける屈折率増大機構の解明

課題番号　12450132

研究組織

研究代表者：大木義路
（早稲田大学理工学部教授）
研究分担者：浜義昌
（早稲田大学理工学総合研究センター教授）
研究分担者：宗田孝之
（早稲田大学理工学部教授）
研究分担者：加藤宙光
（日本学術振興会特別研究員）

研究経費

平成12年度	4,200千円
平成13年度	4,800千円
平成14年度	1,800千円
合計	10,800千円

研究発表

[雑誌論文]

1. T. Nakanishi, Y. Ohki (他4名、5番目) Ultraviolet photon-induced absorption bands and paramagnetic centers in Ge and Sn co-doped SiO_2 glass, J. Non-Cryst., 2003年4月, Vol. 318, 87-94.
2. H. Kato, Y. Ohki (他3名、3番目) Band-tail photoluminescence in hydrogenated amorphous silicon oxynitride and silicon nitride films, to appear in J. Appl. Phys., 2003年1月, Vol. 93, 239-244.
3. K. S. Seol, Y. Ohki (他2名、3番目) Characteristics of Nanoparticles Formed during Pulsed Laser Ablation of $SrBi_2Ta_2O_9$, Jpn. J. Appl. Phys., 2002年9月 Vol. 41, 5654-5658
4. K. S. Seol, Y. Ohki (他4名、6番目) Gas-phase production of monodisperse lead zirconate

titanate nanoparticles, Appl. Phys. Lett., 2002 年 9 月　Vol. 81, 1893-1895

5. H. Ono, Y. Ohki (他 2 名、4 番目) Factors Influencing the Dielectric Properties of Linear Low-Density Polyethylene, Electrical Engineering in Japan, 2002 年 8 月 Vol. 140, 1-7
6. H. Kato, Y. Ohki (他 4 名、6 番目) Plasma-enhanced chemical vapor deposition and characterization of high-permittivity hafnium and zirconium silicate films, J. Appl. Phys., 2002 年 7 月 Vol. 92, 1106-1111
7. T. Yamaguchi, Y. Ohki (他 6 名、6 番目) Evaluation of Silica Glasses Implanted by High-energy Ions Using a UV-excited microspectroscopy, Nuclear Instruments and Methods in Physics Research B, 2002 年　Vol. 191, 371-374
8. M. Hattori, Y. Ohki (他 9 名、3 番目) Characterization of Ion-implanted Silica Glass by Vacuum Ultraviolet Absorption Spectroscopy, Nuclear Instruments and Methods in Physics Research B, 2002 年 Vol. 191, 362-365
9. H. Nishikawa, Y. Ohki (他 7 名、5 番目) Radiation Effects and Surface Deformation of Silica by Ion Microbeam, Nuclear Instruments and Methods in Physics Research B, 2002 年 Vol. 191, 342-345
10. H. Kato, Y. Ohki (他 2 名、4 番目) Photo-induced refractive index change in hydrogenated amorphous silicon oxynitride, J. Appl. Phys., 2002 年 5 月 Vol. 91, 6350-6353
11. R. Ceccato, Y. Ohki (他 7 名、9 番目) Nucleation of Ga_2O_3 Nanocrystals in the K_2O-Ga_2O_3-SiO_2 Glass System, J. Appl. Phys., 2001 年 9 月 Vol. 90, 2522-2527
12. H. Kato, Y. Ohki (他 5 名、7 番目) Visible Electroluminescence in Hydrogenated Amorphous Silicon Oxynitride, J. Appl. Phys., 2001 年 9 月 Vol. 90, 2216-2220
13. R. Ceccato, Y. Ohki (他 7 名、8 番目) Low-wavenumber Raman Scattering Spectroscopy in the Studies of New Gallium-doped Silica Glass-based Transparent Vitroceramic Medium, J. Raman Spectroscopy, 2001 年 8 月 Vol. 32, 643-647
14. T. Noma, Y. Ohki (他 4 名、5 番目) Origin of photoluminescence around 2.6 - 2.9 eV in silicon oxynitride, Applied Physics Letters, 2001 年 9 月 Vol. 79, 1995-1997
15. H. Nishikawa, Y. Ohki (解説)シリカ系フォトニクスガラスの高機能化、電気学会部門誌 A、2001 年 8 月 Vol. 121-A, 721-724
16. H. Kato, Y. Ohki (他 3 名、5 番目) Thermally induced photoluminescence quenching center in hydrogenated amorphous silicon oxynitride, J. Phys. Condens. Matter, 2001 年 7 月 Vol. 13, 6541-6549
17. K. S. Seol, Y. Ohki (他 3 名、3 番目) Low-temperature crystallization induced by excimer laser irradiation of $SrBi_2Ta_2O_9$ films, J. Mater. Res., 2000 年 7 月 Vol. 16. 1883-1886
18. H. Kato, Y. Ohki (他 4 名、4 番目) プラズマ化学気相堆積法によるハフニウムシリケート膜の堆積、放電研究、2001 年 6 月 Vol. 44, 69-73
19. T. Toyoda, Y. Ohki (他 3 名、5 番目) Photoluminescence in Polypropylene Induced by

Ultraviolet Laser Irradiation, UVSOR Activity Report 2000, 2001 年 4 月 110-111

20. T. Toyoda, Y. Ohki (他3名、3番目) Estimation of Conductivity and Permittivity of Water Trees in Polyethylene from Space Charge Distribution Measurements, IEEE Trans. Dielectrics and Electrical Insulation, 2001 年 2 月 Vol. 8, 111-116
21. K. Suzuki, Y. Ohki (他 3 名、 4 番目) Correlation between Space Charge Distribution in Aged XLPE Cable and Location of Water Tree, IEEE Trans. Dielectrics and Electrical Insulation, 2001 年 2 月 Vol. 8, 78-81
22. T. Noma, Y. Ohki (他 4 名、 6 番目) Photoluminescence Analysis of Plasma-deposited Oxygen-rich Silicon Oxynitride Films, Jpn. J. Appl. Phys. Part A, 2000 年 12 月 Vol. 39, 6587-6593
23. M. Fujimaki, Y. Ohki (他 3 名、 3 番目) Ion-implantation-induced densification in silica-based glass for fabrication of optical fiber gratings, J. Appl. Phys, 2000 年 11 月 Vol. 88, 5534-5537
24. K. S. Seol, Y. Ohki (他 3 名、 5 番目) Time-resolved photoluminescence study of hydrogenated amorphous silicon nitride, Phys. Rev. B, 2000 年 7 月 Vol. 1532-1535
25. A. Nakamura, T. Sota, Y. Ohki (他 6 名、 4 番目) Application of Infrared Attenuated Total Reflection Spectroscopy to In-situ Analysis of Atheromatous Plaques in Aorta, Jap. J. Appl. Phys., 2000 年 6 月 Vol. 39, L490-L492
26. H. Kato, Y. Ohki (他 4 名、 6 番目) Photoluminescence in amorphous silicon oxynitride grown by plasma-enhanced chemical vapor deposition, UVSOR Activity Report 1999, 2000 年 4 月
27. K. S. Seol, Y. Ohki (他3名、5番目) Effects of internal post-oxidation on the oxygen deficiency and dielectric strength of buried oxide formed by the separation-by-implanted-oxygen (SIMOX) process, Electrical Engineering in Japan, 2000 年 Vol. 130, 15-20

[国際学会発表]

1. Characterization of Refractive Index Changes of Silica Glass Induced by Ion Microbeam, The 8th International Conference on Nuclear Microprobe Technology and Applications, 2002/9.
2. Characterization of Ion-implanted Silica Glass by Micro-photoluminescence and Raman Spectroscopy, The 8th International Conference on Nuclear Microprobe Technology and Applications, 2002/9.
3. Chemical structures and dielectric properties of hafnium and zirconium silicate films fabricated by plasma enhanced chemical vapor deposition, 2001 Material Research Society Fall Meeting, 2001/11
4. Characterization of hafnium silicate films fabricated by plasma enhanced chemical vapor deposition, 2001 International Symposium on Dry Process, 2001/11.
5. Fabrication of hafnium silicate films by plasma enhanced chemical vapor deposition, 2001 International Symposium on Electrical Insulating Materials, 2001/11.

6. Photoluminescence properties of hydrogenated amorphous silicon nitride films, 2001 International Symposium on Electrical Insulating Materials, 2001/11.
7. Ultraviolet-photon-induced paramagnetic centers in Ge and Sn co-doped silica glass, 2001 International Symposium on Electrical Insulating Materials, 2001/11.
8. Electrical properties in silicon oxynitride and silicon nitride prepared by plasma-enhanced chemical vapor deposition, 2001 International Symposium on Electrical Insulating Materials, 2001/11.
9. Effect of photon irradiation on SBT films, 2001 International Symposium on Electrical Insulating Materials, 2001/11.
10. Characterization of hafnium and zirconium silicate films fabricated by plasma-enhanced chemical vapor deposition, International Workshop on Gate Insulator 2001, 2001/11.
11. Evaluation of Three Dimensional Microstructures on Silica Glass Fabricated by Ion Microbeam, JAERI-Review 2001, TIARA Annual Report 2000, p. 235-237, 2001/10.
12. Characterization of Ion-implanted Silica Glass by Vacuum Ultraviolet Absorption Spectroscopy, 11th International Conference on Radiation Effects in Insulators, 2001/9.
13. Evaluation of Silica Glasses Implanted by High-Energy Ions Using a UV-excited Microspectroscopy 11th International Conference on Radiation Effects in Insulators, 2001/9.
14. Radiation Effects and Surface Deformation of Silica by Ion Microbeam, 11th International Conference on Radiation Effects in Insulators, 2001/9.
15. Low Temperature Crystallization of $SrBi_2Ta_2O_9$ and $YMnO_3$ Ferroelectric Films by Ultraviolet Laser Irradiation, 2000 Dry Process Symposium, 61-66, 2000/11.
16. Electroluminescence in Silicone Oxynitride, 6th IEEE International Conference on Properties and Applications of Dielectric Materials, 2000/6

研究成果による工業所有権の出願・取得状況

工業所有権の名称	発明者名	権利者名	工業所有権の種類、番号	出願年月日
光導波路形成方法及び光導波路	大木義路 加藤宙光 藤巻真 野間崇	大木義路 加藤宙光 藤巻真 野間崇	特願 2001-270151	2001 年 9 月 6 日
耐熱処理装置及び耐熱処理方法並びにグレーティング	大木義路 藤巻真 徳弘真一郎 野村健一 今村一雄	大木義路 藤巻真 徳弘真一郎 野村健一 今村一雄	特願 2000-264328	2000 年 8 月 31 日

研究成果

1.　研 究 目 的

現在、光通信システムは全世界の通信網の機軸をなしている。近年、インターネットトラヒックの急増により、通信ネットワークの大容量化が必要となってきている。その要求を満たすための最も有効な策として、波長の異なる光信号を同時に送る波長多重技術が挙げられる。この技術により、現存する光ファイバ通信網の容量を数十倍にすることが出来るため、新しいインフラを敷設する必要が殆どなくなる。その絶大な有用性より、世界各国の研究機関がその実現のために力を注いでいる。

波長多重通信システムの実現には、複数の信号光の分離のため、光フィルターやミラーといった光ファイバ型光学素子が不可欠となってくる。この目的には、光ファイバコア中に周期的に屈折率変化を誘起することにより形成される光ファイバグレーティングが有効である。これまで、光ファイバグレーティングの形成には、光ファイバコアにおける紫外光誘起屈折率変化が用いられてきた。高効率なグレーティングの作成には、1×10^{-3}程度と非常に大きな屈折率変化量が必要であるため、紫外光感度の高い特殊な Ge 添加シリカガラスをコアとした光ファイバが主として用いられてきた。しかしながら、通常の Ge 添加シリカコア光ファイバでは誘起屈折率変化量は、はるかに小さく、素子作成は困難である。そこで、高圧で水素処理を行いガラスの反応性を高めたり、高濃度の Ge を添加したシリカを用い素子作成が行われてきた。しかしこれらの手法には欠点がある。水素処理の場合、２週間という長い処理時間が要求され、しかも水素の導入により通信帯域でのロスが生じる。高濃度の Ge をコアに添加した場合、コアの屈折率が高くなりすぎ、既存の光ファイバシステムとの接合性が悪くなる。よって、これらの問題点を解消できる新しい光ファイバグレーティング作成技術の開発が必要とされている。本研究は、我々の提案してきた新しい光ファイバグレーティング作成方法の実現可能性を物性学的に明らかにし、実際のグレーティング作成を目指すものである。

2.　研 究 成 果

[2000 年度の成果]

①　顕微分光法によるマイクロビーム照射領域の評価手法の確立：シリカガラスに短冊状に H^+マイクロビーム照射（ビーム径：～1μm）を行い、顕微フォトルミネッセンス（PL）分光により評価した。PL においては波長 650 nm で非架橋酸素正孔（≡Si－O・, "・" は不対電子）による PL 帯が観測された。照射域 1μm 幅に対し、深さ30μm で PL 強度分布が 15μm 程度の広がりを示す。PL の 3 次元分布と TRIM シミュレーションから欠陥生成機構の検討に着手した。

②　光ファイバ形回折格子の形成と評価：マスクを介し光ファイバに H^+注入することにより作製したシリカコア光ファイバへの回折格子の透過光スペクトルを調べた。1300nm 付近に透過光損失を有するフィルター素子が形成された。しかし、クラッド部分にも屈折率変

化が誘起され1300nm以外での波長域での損失も大きい。そこで、クラッド部の損失を低減し素子の高品質化を図るため、マイクロビームによるコア部への局部的照射を試みた。マイラーフィルムを介した照射の場合、エネルギー2.47MeVでH^+が光ファイバのコア部に達し、屈折率の上昇が確認された。以上により、光ファイバ回折格子形成の最適照射条件を得た。また、屈折率上昇のメカニズムについて、理論的検討を加えた。

[2001年度の成果]

① マイクロイオンビーム照射による欠陥生成： H^+マイクロイオンビーム（ビーム径：1 μm）照射によりシリカガラス中に誘起される欠陥の生成機構を顕微フォトルミネッセンス、顕微ラマン分光、および電子スピン共鳴法により評価した。注入H^+イオンの通過による正常結合の切断によって、E' center（O≡Si・, "・"は不対電子）や非架橋酸素孔子（≡Si－O・）等の欠陥が生じる。これら欠陥の生成効率は、シリカガラス中のOH基の有無に強く影響される。注入イオンのエネルギー損失過程において、原子衝突よりも電子励起の効果が大きいことをTRIMシミュレーションにより明らかにした。さらに、マイクロイオンビームを用いて光ファイバ中に周期構造を実際に形成し、透過光損失特性の評価に着手した。

② 紫外光照射による屈折率増大： 屈折率を1.45－2.00まで自在に変化できるシリコン酸窒化物は、光導波路材料の一つとして考えられている。紫外光エキシマレーザを照射することにより、屈折率を増加させることの可能なシリコン酸窒化物の作成方法および組成を明らかにした。紫外光照射により誘起されるラジカル欠陥種の同定および定量を電子スピン共鳴法により行い、屈折率の変化量をエリプソメータにより見積もった。屈折率上昇のメカニズムとして、高密度化に因る効果が70-98 %の割合を占め、ラジカル欠陥生成に因る光吸収増加の効果は数%程度であることを計算により導いた。さらに、周期1 μmの平面回折格子を位相格子法により実際に作成し、光加工性の良さを示した。

[2002年度の成果]

① イオンマイクロビーム照射によるシリカガラスの高密度化と屈折率変化： H^+イオンマイクロビーム照射によるシリカガラスの形状および屈折率の変化を原子間力顕微鏡、顕微ラマン分光装置および二光束干渉顕微鏡を用いて調べた。イオンマイクロビーム照射されたシリカガラスの表面および側面ともにイオン注入により凹みが観測され、その主たる原因は高密度化であるということを明らかにした。高密度化が生じると屈折率は増加することが知られているが、イオン注入誘起屈折率変化は飛程付近で最大となり、回折格子作製に十分な値である5.9×10^{-3}まで達することが分かった。

② イオン注入マスクを用いた光通信用素子作成技術： イオン注入マスクとして、電子線リソグラフィーにより、Si_3N_4メンブレン上にレジストと金から構成される周期 2.65 μmの Line/Space パターンを作製した。作製したマスクを用いてイオン注入をシリカガラスに

行うと、レジストと金の阻止能の違いから注入イオンの飛程に差がでる。HF でエッチングを行い、飛程の差に起因する凹凸の回折格子が形成された。この領域に He-Ne レーザ光を照射するとフラウンホーファー回折による+1 次光および-1 次光を観察することができた。これら高次光の出射角より、回折格子の周期は 2.6 μm であると計算された。この値はイオン注入マスクの Line/Space の周期と一致し、イオン注入マスクパターン転写の成功が裏付けられた。

[3 年間の成果のまとめ]

① イオンマイクロビーム照射によるシリカガラスの高密度化と屈折率変化：シリカガラスに H^+マイクロビーム照射を行い、顕微フォトルミネッセンス・ラマン分光、電子スピン共鳴法により評価した。注入イオンのエネルギー損失には原子衝突よりも電子励起の効果が大きいことをシミュレーションにより明らかにした。さらに、光ファイバ中に周期構造を実際に形成し、透過光損失特性を評価した。イオン照射されたシリカガラスの表面および側面に凹みが観測され、その主原因は高密度化であることを明らかにした。誘起屈折率変化は飛程付近で最大となり、回折格子作製に十分な値まで達することが分かった。マスクとして、電子線リソグラフィーによりシリコン窒化膜メンブレン上に周期 2.65 マイクロメートルの Line/Space パターンを作製し、イオン注入を行ったのちエッチングを行い、飛程の差に起因する凹凸の回折格子を形成した。フラウンホーファー回折により、回折格子の周期は Line/Space の周期と同じであると計算され、マスクパターン転写の成功が裏付けられた。

② 紫外光照射による屈折率増大： 屈折率を 1.45－2.00 まで自在に変化できるシリコン酸窒化物は、光導波路材料の一つとして考えられている。紫外光エキシマレーザを照射することにより、屈折率を増加させることの可能なシリコン酸窒化物の作成方法および組成を明らかにした。屈折率上昇のメカニズムとして、高密度化に因る効果が大きいことを計算により導いた。さらに、周期 1 μm の平面回折格子を位相格子法により実際に作成し、光加工性の良さを示した。

研究成果の詳細

JOURNAL OF APPLIED PHYSICS VOLUME 90, NUMBER 5 1 SEPTEMBER 2001

Visible electroluminescence in hydrogenated amorphous silicon oxynitride

Hiromitsu Kato,[a),b)] Akira Masuzawa, and Hidefumi Sato
Department of Electrical, Electronics, and Computer Engineering, Waseda University, Shinjuku-ku 169-8555, Japan

Takashi Noma
Advanced Research Institute for Science and Engineering, Waseda University, Shinjuku-ku 169-8555, Japan and Engineering Department 1, System-LSI Division, Sanyo Electric Co. Ltd., Oizumi-Machi 370-0596, Japan

Kwang Soo Seol
Advanced Research Institute for Science and Engineering, Waseda University, Shinjuku-ku 169-8555, Japan and RIKEN (The Institute of Physical and Chemical Research), Wako 351-0198, Japan

Makoto Fujimaki
Advanced Research Institute for Science and Engineering, Waseda University, Shinjuku-ku 169-8555, Japan and Optical Radiation Section, Electrotechnical Laboratory, Tsukuba 305-8568, Japan

Yoshimichi Ohki
Department of Electrical, Electronics, and Computer Engineering, Waseda University, Shinjuku-ku 169-8555, Japan and Advanced Research Institute for Science and Engineering, Waseda University, Shinjuku-ku 169-8555, Japan

(Received 22 November 2000; accepted for publication 4 June 2001)

The mechanism of electroluminescence in hydrogenated amorphous silicon oxynitride was investigated. The luminescence can be observed only in the samples with high nitrogen content and annealed at high temperatures. It depends on the direction of the applied electric field, and its peak photon energy decreases from 2.3 to 1.8 eV as the nitrogen content increases. From the measurements of conduction current and Fourier transform infrared absorption spectroscopy, it was found that the electrical conduction in the electric field region where the luminescence was observed is governed by the Poole–Frenkel process at the defect centers induced by the high temperature annealing. The electroluminescence is considered to be caused by electronic transition between the band-tail states, at least one of which is related to N or Si–N bonds. © *2001 American Institute of Physics.* [DOI: 10.1063/1.1388864]

I. INTRODUCTION

Hydrogenated amorphous silicon oxynitride (a-SiO_xN_y:H) is one of the most important insulating materials in microelectronics, and much research has been carried out.[1–4] It has a possibility of realizing an excellent electronic property similar to silicon dioxide while keeping a high permittivity value of silicon nitride by choosing a proper composition of y/x.[5–8] Since its refractive index can be controlled by changing the y/x ratio, it also has a possible application to optical fibers[9] and waveguides.[10] Moreover, luminescence of this material has been reported by several authors,[11–15] which may open the door for its application to all-Si-based optoelectronics technology. The present article reports a visible electroluminescence (EL) of a-SiO_xN_y:H. The EL energy changes from red to yellow depending on the nitrogen content, which is attractive for optoelectronics. The EL mechanism is also discussed based on the results of conduction current measurement and Fourier transform infrared (FTIR) absorption spectroscopy.

II. EXPERIMENTAL PROCEDURES

The a-SiO_xN_y:H films were deposited on a p-type (100) silicon monocrystal substrate by plasma enhanced chemical vapor deposition (PECVD) using a mixture of SiH_4, N_2O, and N_2 gases. The substrate temperature was 400 °C and the plasma frequency was 13.56 MHz. By changing the flow rate of SiH_4, five types of films with different nitrogen contents were prepared as shown in Table I. The elementary compositions of Si, O, and N were estimated through x-ray photoelectron spectroscopy (JEOL JPS-90MX). The thickness and refractive index measured by ellipsometry (ULVAC ESM-1) are also shown in Table I.

For annealing, the samples were kept at a temperature ranging from 500 to 900 °C in vacuum (3.0×10^{-2} Pa) with a rapid thermal annealing apparatus for 10 min. The chemical change induced was examined by FTIR absorption spectroscopy (JEOL JIR-WINSPEC50). The electrical properties were examined by measuring the conduction current using a high resistance meter (Advantest R8340) and the capacitance–voltage characteristics at 1 MHz using a HF C–V meter (Sanwa Mega Bytek MI-494) for the sample having evaporated gold electrodes with an effective area of 7.9 $\times10^{-3}$ cm^2. In the EL measurements, a semitransparent gold electrode with an effective area of 4.0×10^{-1} cm^2 and a

[a)]Electronic mail: 600c5050@mn.waseda.ac.jp
[b)]Research Fellow of the Japan Society for the Promotion of Science.

 © 2001 American Institute of Physics

TABLE I. Elementary composition, refractive index, and thickness of a-SiO_xN_y:H films tested.

Sample	at. %			N/O	Empirical formula	Refractive index	Thickness (nm)
	Si	O	N				
A	35	62	3.6	5.8×10^{-2}	$SiO_{1.8}N_{0.10}$	1.49	117
B	35	59	6.0	1.0×10^{-1}	$SiO_{1.7}N_{0.17}$	1.53	117
C	35	57	7.0	1.2×10^{-1}	$SiO_{1.6}N_{0.20}$	1.57	117
D	37	56	7.7	1.4×10^{-1}	$SiO_{1.5}N_{0.21}$	1.62	114
E	38	53	9.6	1.8×10^{-1}	$SiO_{1.4}N_{0.26}$	1.67	112

transmittance of about 30% was vacuum evaporated as the upper electrode. Photoluminescence (PL) was measured under excitation by a KrF excimer laser (wavelength: 248 nm =5.0 eV; pulse width: ~25 ns; pulse energy: ~300 mJ/cm^2, Lambda Physik COMPEX205). These luminescence spectra were measured at room temperature using a monochromator (Jobin-Yvon HR320) equipped with an intensified charge coupled device array (Princeton Instruments ICCD-576G/RBT).

III. RESULTS AND DISCUSSION

Figure 1 shows PL spectra observed in the unannealed samples excited by the KrF excimer laser. As reported in our previous paper,[12] samples A and B have PL bands with their peaks at 2.7 and 4.4 eV (not shown), originated from silicon homobonds (Si–Si) in SiO_2,[16,17] while the PL observed in samples C–E, which changes its peak energy from 2.8 to 2.3 eV with an increase in the nitrogen content is attributable to radiative recombination of electron–hole pairs between localized states located below the conduction band and above the valence band, either or both of which being associated with N or Si–N bonds. This attribution is based on the following facts. The PL is considered to be due to radiative recombination between localized states in many materials similar to the present sample such as a-Si:H,[18] a-SiN_x:H,[19,20] and a-SiC_x:H.[21] Especially, the PL in a-SiN_x:H and the present PL are quite similar.[12]

The present PL spectra are broad. The temperature dependence of PL characteristics was measured from 10 to 300 K. The full width at half maximum of the PL band is constant at ~0.8 eV within the temperature region. This excludes the possibility that the broad PL is due to a thermal effect. The broadness of PL spectra most likely suggests that the localized states are distributed widely, resulting in a long-lasting band edge. This is often observed in amorphous materials.[18–21] The PL peak moves toward red with an increase in the nitrogen content, as is clearly seen by comparing PL spectra among samples C–E. This is probably because the forbidden gap energy becomes narrow.[12,13] The peak energy further shifts by thermal annealing as will be explained later. Therefore we call this PL the 2.2–2.9 eV PL in the present article. Note that the 2.7 eV PL in samples A and B and the 2.2–2.9 eV PL in samples C–E are totally different PLs with significantly different decay constants.[12]

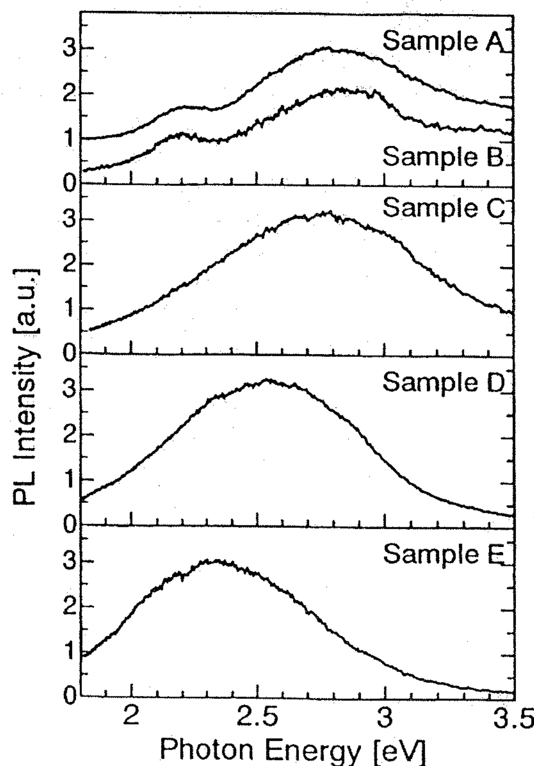

FIG. 1. PL spectra observed in the unannealed samples A–E excited at 5.0 eV.

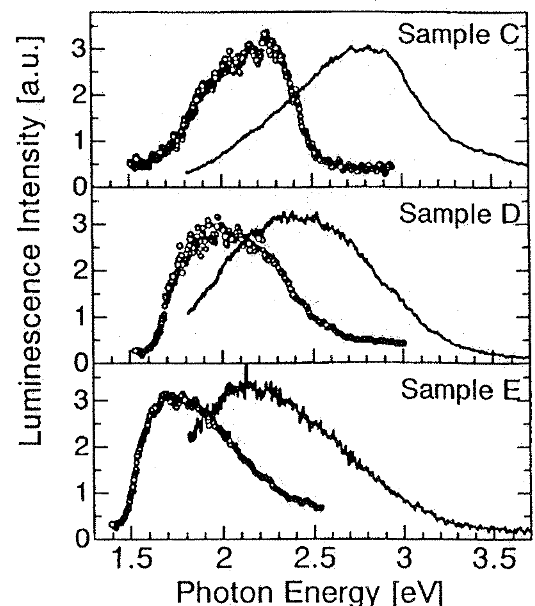

FIG. 2. EL spectra (denoted by open circles) and PL spectra (solid curves) in samples C–E annealed at 900 °C.

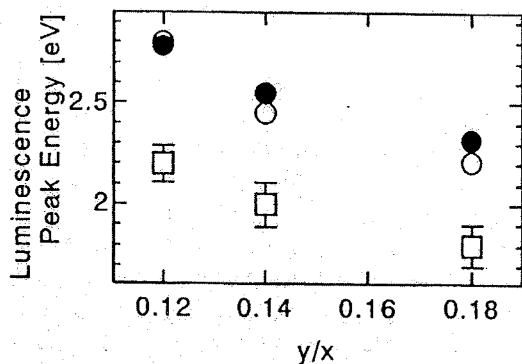

FIG. 3. Relation between the nitrogen content (N/O or y/x in SiO_xN_y:H) and the peak position of luminescence. Closed circles are for the PL in the unannealed samples, open circles are for the PL in the samples annealed at 900 °C, and squares are for the EL in the annealed samples.

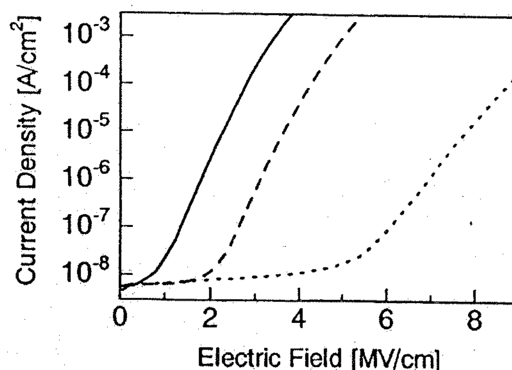

FIG. 5. Electric field dependence of conduction current density obtained for samples annealed at 900 °C. Dotted, broken, and solid lines are for samples C–E, respectively.

We tried to obtain similar EL spectra of the samples, but no EL appeared. Then, the samples were thermally annealed, and it was found that EL appeared only in the annealed samples C–E. Open circles in Fig. 2 show the EL spectra observed in the samples annealed at 900 °C. The peak energy decreases with an increase in the nitrogen content from 2.3 eV in sample C to 1.8 eV in sample E. The lowest annealing temperature necessary to observe EL is different among the samples, and is 800 °C in sample C, 700 °C in sample D, and 600 °C in sample E.

Solid curves in Fig. 2 show PL spectra in the samples annealed at 900 °C. Similarly to the unannealed samples, the 2.2–2.9 eV PL is observed in samples C–E, and the shift of its peak energy is also similar to the unannealed samples. In the case of annealed samples C–E, the EL peak also shows a similar shift. Figure 3 compares the peak shift among EL and PL in the annealed samples and the PL in the unannealed samples, which clearly shows a similarity among the three peak shifts, even though the peak positions are different. It is considered that the peak shift is due to the decrease in the band gap energy with an increase in the nitrogen content. The fact that both the EL and the 2.2–2.9 eV PL are observed in the same samples with a similar tendency of peak shift suggests that the same radiation process is involved in the two luminescence mechanisms.

The EL is observed only under the forward bias condition when the polarity of the p-type silicon is positive. Figure 4 shows the relationship between the applied electric field and EL intensity of sample E annealed at 900 °C. The conduction current density measured under the same condition is also shown. The EL intensity and the current density become larger in quite similar manners with an increase in the applied electric field. This indicates that the conduction carriers play an important role in EL. The electric field, where the EL becomes observable, is about 6, 4, and 3 MV/cm in samples C–E, respectively. The peak energy did not depend on the electric field intensity.

Figure 5 shows the relation between the current density and the electric field intensity observed in samples C–E annealed at 900 °C. The tunneling effect, the Schottky effect, and the Poole–Frenkel (PF) effect are known to be typical high-field conduction mechanisms.[22–26] Figure 6 shows the PF plots drawn based on the data shown in Fig. 5. Here J and E represent the current density and electric field intensity, respectively. The PF plots give straight lines, while the other two effects did not give straight lines. The permittivity is calculated to be 4.6, 5.2, and 6.3 for samples C–E, respectively, from the slopes of PF plots. These values are close to the respective permittivity values, 3.9, 4.1, and 4.5 for the

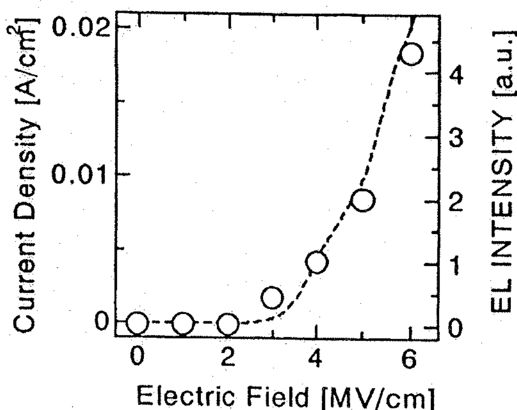

FIG. 4. The EL intensity (circles) and the conduction current density (broken curve) in sample E annealed at 900 °C as a function of electric field intensity.

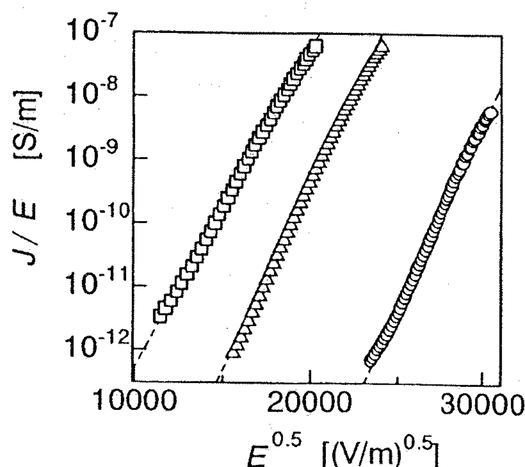

FIG. 6. Poole–Frenkel plots. The current density and electric field intensity are denoted by J and E, respectively. Circles, triangles, and squares indicate the data obtained for samples C–E annealed at 900 °C, respectively.

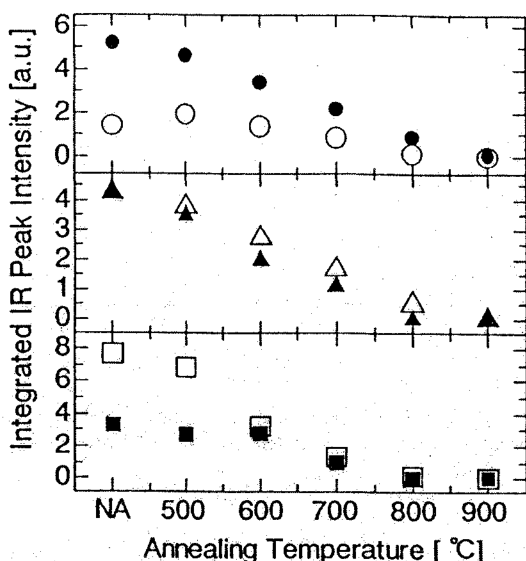

FIG. 7. Change in IR absorption intensities due to the Si–H mode at 2200 cm^{-1} (denoted by open symbols) and the N–H mode at 3340 cm^{-1} (closed symbols) induced by the thermal annealing. Circles, triangles, and squares indicate the data obtained for samples C–E, respectively. NA: not annealed.

annealed samples C–E, calculated from the capacitance values measured as a function of voltage. From these results it is considered that the conduction is governed by the PF process when the EL appears. This is reasonable because it is generally accepted that the high-field conduction is dominated by the PF process in silicon nitride and silicon oxynitride.[26]

For the EL observed in silicon oxide,[27,28] silicon nitride,[29] and silicon oxynitride[14,15] with a metal–insulator–semiconductor structure, two models have been proposed. One is the hot carrier model, where electrons and holes are assumed to be accelerated significantly so that they can run close to the conduction and valence bands.[27] In the other model, i.e., in the injection model, while electrons and holes are assumed to be injected from electrodes, no further significant acceleration is postulated.[14,15,28,29] If the carriers in the present samples are generated by the PF effect and are transported by a hopping process, it is difficult to assume that they are accelerated so much. The carriers are thought to be

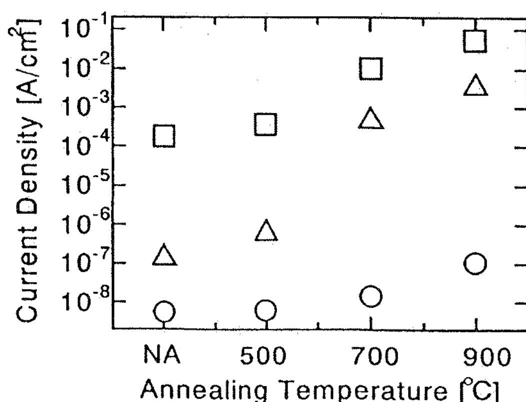

FIG. 8. Relationship between the annealing temperature and the current density measured at 6 MV/cm. Circles, triangles, and squares indicate the data obtained for samples C–E, respectively. NA: not annealed.

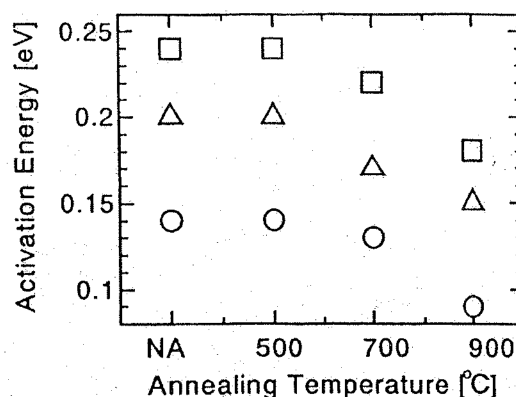

FIG. 9. Activation energy as a function of the annealing temperature. Circles, triangles, and squares indicate the data obtained for samples C–E, respectively. NA: not annealed.

barely transported via the PF sites, holding the minimum necessary energy. However, in the case of PL, electrons excited by UV photons to a level much higher than the bottom of the conduction band can contribute to the PL. Therefore the energy of photons emitted in EL should coincide with the lowest energy of photons emitted in PL. This is clearly demonstrated if we compare the EL spectra and the PL spectra shown in Fig. 2. Note that the PL in samples A and B originates from silicon homobonds as mentioned above and is out of the present discussion. When the *p*-type silicon is positively biased, holes are easily injected into the a-SiO_xN_y:H layer, while electrons can be injected from the gold electrode. The injected electrons and holes are transported through the localized PF sites to luminescence centers where they recombine with each other, releasing the excess energy. This is considered to be the mechanism of EL.

Next, the effect of thermal annealing is discussed. The IR spectroscopy measurements revealed that the present samples have absorption peaks around 1000, 2200, and 3340 cm^{-1}, which are attributable to the superposition of Si–O and Si–N stretching, Si–H stretching, and N–H stretching, respectively.[30] Figure 7 shows the change in the IR absorption intensities due to the N–H and Si–H modes observed in samples C–E. These intensities decrease with an increase in the annealing temperature. In the case of silicon nitride, it has been reported that the Si–H and N–H bonds are broken at high temperatures and that H_2 molecules come out of the material.[19,31] It is considered that hydrogen is also released from the present silicon oxynitride sample by the annealing. If the hydrogen terminating imperfections such as dangling bonds come out, many defect states will appear within the forbidden gap.

Figure 8 shows the relation between the annealing temperature and the current density for samples C–E measured at 6 MV/cm. The current density increases with an increase in the annealing temperature. Figure 9 shows the activation energy estimated from the measurement temperature dependence of current density as a function of the annealing temperature obtained for samples C–E. The activation energy decreases with an increase in the annealing temperature. If the annealing beyond 500 °C induces hopping sites, the activation energy becomes smaller and the conduction current

becomes larger. This helps electrons and holes reach the luminescence centers and recombine there with each other.

Finally, we would add a few words about the luminescence centers. There have been papers[11,14] reporting that the EL and the PL in silicon oxynitride are due to Si–Si or Si–H bonds. However, as shown in Fig. 7, Si–H bonds disappear when the EL appears. As mentioned above, we have already discarded the possibility of the PL being due to Si–Si bonds, mainly from a clear difference in the PL decay constant between the two origins.[12] The PL around 2.7 eV originated from the Si–Si bonds has a decay constant as slow as 10 ms, while the PL around 2.6–2.9 eV in silicon oxynitride has a decay constant as fast as 3.7 ns.[12] Unfortunately, no such clear judgment can be done for EL, since it is virtually impossible to measure its decay constant. However, the EL peak energy is related to the nitrogen content as shown in Fig. 3 and the EL was observed only in the samples for which the 2.2–2.9 eV PL is the only PL at least in the energy region around there. Therefore it is highly probable that the EL luminescence center is associated with Si–N bonds.

IV. CONCLUSION

The a-SiO_xN_y:H films ($1.4<x<1.6$, $0.20<y<0.26$) deposited by PECVD exhibit EL around 1.8–2.3 eV after they were thermally annealed. The EL is attributable to the recombination between the localized states associated with Si–N bonds located below the conduction band and above the valence band. The annealing induces many carrier transport centers that help electrons and holes reach the localized states.

[1] M. Murata, K. Yamauchi, H. Kojima, A. Yokoyama, T. Inoue, and T. Iwamori, J. Electrochem. Soc. **140**, 2346 (1993).
[2] H. Fukuda, T. Arakawa, and S. Ohno, Electron. Lett. **26**, 1505 (1990).
[3] M. Bhat, L. K. Han, D. Wristers, J. Yan, and D. L. Kwong, Appl. Phys. Lett. **66**, 1225 (1995).
[4] T. Ito, T. Nakamura, and H. Ishikawa, IEEE Trans. Electron Devices **ED-29**, 498 (1982).
[5] V. J. Kapoor, R. S. Bailey, and R. A. Turi, J. Electrochem. Soc. **137**, 3589 (1990).
[6] A. Hashimoto, M. Kobayashi, T. Kamijoh, H. Takano, and M. Sakuta, J. Electrochem. Soc. **133**, 1464 (1986).
[7] M. Bhat, J. Kim, J. Yan, G. W. Yoon, L. K. Han, and D. L. Kwong, IEEE Electron Device Lett. **EDL-15**, 421 (1994).
[8] Z. Q. Yao, H. B. Harrison, S. Dimitrijev, and Y. T. Yeow, IEEE Electron Device Lett. **EDL-15**, 516 (1994).
[9] G. Chollon, U. Vogt, and K. Berroth, J. Mater. Sci. **33**, 1529 (1998).
[10] T. S. Larsen and O. Leistiko, J. Electrochem. Soc. **144**, 1505 (1997).
[11] K. J. Price, L. E. McNeil, A. Suvkanov, E. A. Irene, P. J. MacFarlane, and M. E. Zvanut, J. Appl. Phys. **86**, 2628 (1999).
[12] T. Noma, K. S. Seol, M. Fujimaki, H. Kato, T. Watanabe, and Y. Ohki, Jpn. J. Appl. Phys., Part 1 **39**, 6587 (2000).
[13] C. Ance, F. d. Chelle, J. P. Ferraton, G. Leveque, P. Ordejon, and F. Yndurain, Appl. Phys. Lett. **60**, 1399 (1992).
[14] K. J. Price, L. R. Sharpe, L. E. McNeil, and E. A. Irene, J. Appl. Phys. **86**, 2638 (1999).
[15] G. F. Bai, Y. P. Qiao, Z. C. Ma, W. H. Zong, and G. G. Qin, Appl. Phys. Lett. **72**, 3408 (1998).
[16] K. S. Seol, Y. Ohki, H. Nishikawa, and Y. Hama, J. Appl. Phys. **80**, 6444 (1996).
[17] K. S. Seol, M. Fujimaki, Y. Ohki, and H. Nishikawa, Phys. Rev. B **59**, 1590 (1999).
[18] R. A. Street, Adv. Phys. **30**, 593 (1981).
[19] K. S. Seol, T. Futami, T. Watanabe, Y. Ohki, and M. Takiyama, J. Appl. Phys. **85**, 6746 (1999).
[20] K. S. Seol, T. Watanabe, M. Fujimaki, H. Kato, Y. Ohki, and M. Takiyama, Phys. Rev. B **62**, 1532 (2000).
[21] W. Siebert, R. Carius, W. Fuhs, and K. Jahn, Phys. Status Solidi B **140**, 311 (1987).
[22] G. P. Kennedy, O. Buiu, and S. Taylor, J. Appl. Phys. **85**, 3319 (1999).
[23] B. L. Yang, H. Wong, and Y. C. Cheng, Solid-State Electron. **37**, 481 (1994).
[24] S. Kimura and H. Ikoma, J. Appl. Phys. **85**, 551 (1999).
[25] T. K. Nguyen, L. M. Landsberger, S. Belkouch, and C. Jean, J. Electrochem. Soc. **144**, 3299 (1997).
[26] B. M. Tao, D. Park, S. N. Mohammad, D. Li, A. E. Botchkerav, and H. Morkoc, Philos. Mag. B **73**, 723 (1996).
[27] D. J. DiMaria, J. R. Kirtley, E. J. Pakulis, D. W. Dong, T. S. Kuan, F. L. Pesavento, T. N. Theis, J. A. Cutro, and S. D. Brorson, J. Appl. Phys. **56**, 401 (1984).
[28] J. Yuan and D. Haneman, J. Appl. Phys. **86**, 2358 (1999).
[29] W. Boonkosum, D. Kruangam, and S. Panyakeow, Jpn. J. Appl. Phys., Part 1 **32**, 1534 (1993).
[30] W. A. P. Claassen, H. A. J. Th. v. d. Pol, A. H. Goemans, and A. E. T. Kuiper, J. Electrochem. Soc. **133**, 1458 (1986).
[31] K. C. Lin and S. C. Lee, J. Appl. Phys. **72**, 5474 (1992).

APPLIED PHYSICS LETTERS VOLUME 79, NUMBER 13 24 SEPTEMBER 2001

Origin of photoluminescence around 2.6–2.9 eV in silicon oxynitride

Takashi Noma[a),b)]
Engineering Department 1, System-LSI Division, Sanyo Electric Company Ltd., Oizumi-Machi 370-0596, Japan

Kwang Soo Seol[a)]
RIKEN (The Institute of Physical and Chemical Research), Wako-shi 351-0198, Japan

Hiromitsu Kato
Department of Electrical, Electronics, and Computer Engineering, Waseda University, Shinjuku-ku 169-8555, Japan

Makoto Fujimaki[a)]
Optical Radiation Section, Electrotechnical Laboratory, Tsukuba 305-8568, Japan

Yoshimichi Ohki[a)]
Department of Electrical, Electronics, and Computer Engineering, Waseda University, Shinjuku-ku 169-8555, Japan

(Received 6 November 2000; accepted for publication 27 July 2001)

A broad photoluminescence (PL) around 2.6–2.9 eV is known to appear in hydrogenated silicon oxynitride. Although its origin was reported to be Si–N bonds, it is not so clear since the material contains hydrogen. In the present research, we have confirmed that the same PL appears in silicon oxynitride grown by nitriding of silicon dioxide. The depth profile of the PL intensity agrees with that of the nitrogen concentration. Furthermore, the emission spectrum, excitation spectrum, and decay constant of this PL agree with those of the PL observed in silicon nitride. Based on these results and theoretical discussion, the origin of the 2.6–2.9 eV PL is estimated to be Si–N bonds.
© *2001 American Institute of Physics.* [DOI: 10.1063/1.1405806]

With the scale reduction of very-large-scale-integrated (VLSI) circuits, a gate insulator with a high permittivity and a high reliability is required. Amorphous-silicon-oxynitride film obtained by thermal nitriding of silicon thermal oxide film is attracting much attention as a strong candidate for the gate insulator. The film has been known to possess a superior resistance to high electric field compared with the silicon thermal oxide. On the other hand, hydrogenated amorphous-silicon-oxynitride film is widely used in VLSI circuits as an interlevel dielectric layer or as a passivation layer. Much research has recently been done on these silicon-oxynitride films in order to reveal the role of incorporated nitrogen by x-ray photoelectron spectroscopy (XPS),[1–3] secondary ion mass spectroscopy,[4,5] infrared absorption,[6] optical absorption,[7] and defect analysis.[8] However, the knowledge is not sufficient to understand the film structure.

We have shown that photoluminescence (PL) is powerful to investigate the localized bonding states in silicon oxide,[9–11] silicon nitride,[12,13] and silicon oxynitride.[14] In hydrogenated amorphous-silicon-oxynitride film deposited by plasma-enhanced chemical-vapor deposition using SiH_4, N_2O, and N_2 as monomer gases, PL appears at 2.7 eV and around 2.6–2.9 eV. The PL at 2.7 eV is clearly due to silicon homobonds, while the broad PL around 2.6–2.9 eV has been attributed to Si–N bonds.[14] However, in a strict sense, this latter assignment has not been well proved since the film consists of four elements, Si, O, N, and H. Therefore, we have prepared silicon oxynitride that consists only Si, O, and N. If the PL mechanism becomes clear, it should help clarify the structure of localized states in these oxynitrides, which in turn, helps improve their electrical properties and reliability as a gate insulator.

The samples are silicon oxynitride grown by the following dry process, and do not include hydrogen. A *p*-type silicon monocrystal wafer was oxidized in O_2 at 1000 °C for 40 s to obtain a silicon-oxide film with a thickness of 5.2 nm, which was then nitrided in NO at 1050 °C for 60 s in a rapid thermal annealing apparatus. The thickness of the grown oxynitride film measured by ellipsometry was 5.8 nm by assuming the refractive index of the film to be 1.46. The concentrations of silicon, oxygen, and nitrogen were measured by Auger electron spectroscopy [(AES), ANELVA, EMAS-II] with a depth resolution of 1.0 nm, while their depth profiles were observed by etching the sample by Ar-ion sputtering (5 kV and 10 mA). The binding energy of N 1*s* electrons was obtained by XPS (JEOL JPS-90MX) with Mg $K\alpha$ x rays, and its depth profile was measured by Ar-ion sputtering. The PL spectrum was measured at room temperature under excitation of a KrF excimer laser (wavelength: 248 nm=5 eV, pulse width: ~20 ns, Lambda Physik LPX105i). The PL excitation (PLE) spectrum and the decay profile were measured at 14 K using synchrotron radiation (SR) at the BL7B line of the UVSOR Facility (Institute for Molecular Science, Okazaki, Japan). The depth profile of the PL intensity was obtained by chemically thinning the film in a HF solution, and the accuracy of the etched thickness measured by ellipsometry was within 0.2 nm.

Figure 1 shows the concentration of nitrogen as a func-

[a)]Also at: Advanced Research Institute for Science and Engineering, Waseda University, Shinjuku-ku 169-8555, Japan.
[b)]Electronic mail: NOMAO79814@swan.sanyo.co.jp

 © 2001 American Institute of Physics

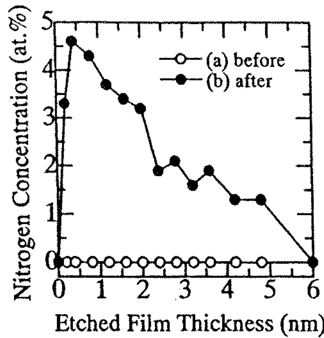

FIG. 1. Concentration of nitrogen as a function of the distance from the sample surface obtained in the film before (a) and after (b) the nitriding.

tion of the distance from the surface obtained by AES in the film before and after the NO nitriding. It is clear that nitrogen is not present in the film before the nitriding. Figure 2 shows the binding energy of N 1*s* electrons as a function of the film thickness etched by Ar sputtering. The peak energy decreases from 398.3 to 397.3 eV with an increase in the etched thickness, excepting the value at the original surface. The binding energy of 397.3 eV is observed in silicon nitride with a refractive index of 2.00, while the one of 398.3 eV is observed in silicon oxynitride with a refractive index of 1.61.[15] In recent papers, the 397.3 eV peak is attributed to N combined with three Si atoms, while the 398.3 eV peak is considered to be due to N bonded with two Si atoms and affected by the presence of O.[1,3] These results show that rapid thermal NO nitriding introduces N atoms bonded to at least two Si atoms throughout the film.

Figure 3(a) shows PL spectra observed in the silicon oxide and the silicon oxynitride, that is, those observed in the film before and after nitriding. While no PL band was observed before the nitriding, a broad PL band around 2.6–2.9 eV appeared afterward. Note that this is a PL report on silicon oxynitride with a thickness as thin as 5.8 nm. The PLE spectrum monitored at 2.8 eV for the PL observed in the nitrided film shown in Fig. 3(b) indicates that the PL was excited by photons with energies higher than 5.0 eV. The PL showed an exponential decay with a lifetime of about 4.2 ns. These properties of the PL are similar to those of the PL observed in hydrogenated silicon nitride (PL peak: about 2.4 eV, PLE peak: >4.5 eV, lifetime 3.2 ns),[12,13] and those observed in hydrogenated silicon oxynitride (PL peak: 2.6–2.9 eV, PLE peak: >4.0 eV, lifetime 3.7 ns).[14] Therefore, PLs in the three materials are considered to be due to the same origin.

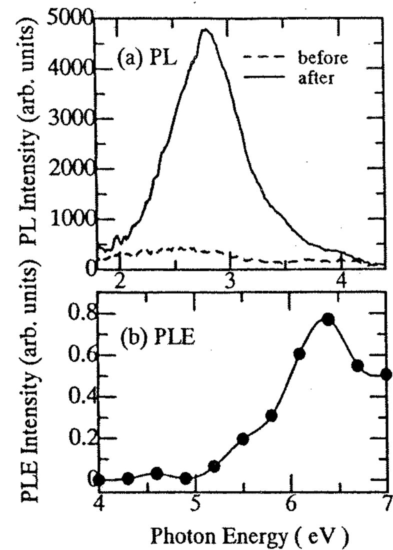

FIG. 3. PL spectra (a) before and after the nitriding and PLE spectrum (b) monitored at 2.8 eV for the PL observed in the nitrided film.

In our previous paper,[14] we reported the similarity between the PL in the hydrogenated silicon nitride and the one in the hydrogenated silicon oxynitride and assumed that Si–N bonds are the PL origin based on the results of XPS, infrared absorption spectroscopy, and electron spin resonance. Although this assignment was well proved experimentally, one weak point is that the sample had a rather complex structure, consisting of hydrogen in addition to the basic elements, Si, O, and N, for silicon oxynitride.

The present film, silicon oxynitride grown with the dry process, does not have hydrogen in its structure. This clearly excludes the possibility of hydrogen being associated with the PL origin. Furthermore, the fact that the PL does not appear before the nitriding, as shown in Fig. 3(a), indicates that the PL is due to the structure induced by the nitriding. Figure 4 shows the PL intensity measured in the remaining film after being etched and the calculated concentration of N present using the data shown in Fig. 1. The two curves are very similar, indicating that the origin of the PL is closely related to N.

According to theoretical calculations,[7,16] Si–N bonds in SiO_2 introduce localized states due to N 2*p* lone pair electrons above the O 2*p* lone pair states at the top of the valence band, which are active in hole trapping and transport. More-

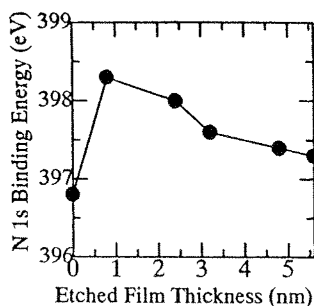

FIG. 2. Binding energy of N 1*s* electrons as a function of the etched film thickness.

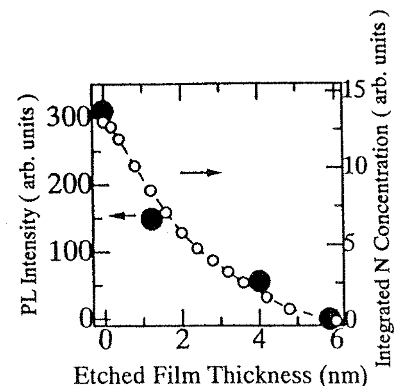

FIG. 4. PL intensity measured in the remaining film after being etched and the integrated concentration of nitrogen present.

over, the top of the valence band is formed by N 2*p* lone pair states in SiO_xN_y with a high-Si–N concentration. This supports the assumption that the 2.6–2.9 eV PL is due to recombination of holes and electrons in localized states associated with Si–N bonds.

In summary, we have confirmed that PL at 2.6–2.9 eV is observed in silicon oxide only after NO nitriding. Based on the instrumental analyses by AES and XPS, theoretical calculations, and the similarity of the properties between the PLs observed in the present film and silicon nitride, it is considered that the origin of the present 2.6–2.9 eV PL is Si–N bonds.

This work was partly supported by the Joint Studies Program (1999) of UVSOR Facility, Institute for Molecular Science, Okazaki, Japan. The authors express their thanks to T. Tabata, T. Kubota, M. Hara, and H. Dobashi of Sanyo Electric Co. Ltd., and T. Koizumi of the Research Support Section, Waseda University for their cooperation.

[1] Z. H. Lu, S. P. Tay, R. Cao, and P. Pianetta, Appl. Phys. Lett. **67**, 2836 (1995).
[2] E. C. Carr, K. A. Ellis, and R. A. Buhrman, Appl. Phys. Lett. **66**, 1492 (1995).
[3] E. C. Carr and R. A. Buhrman, Appl. Phys. Lett. **63**, 54 (1993).
[4] N. S. Saks, D. I. Ma, and W. B. Fowler, Appl. Phys. Lett. **67**, 374 (1995).
[5] P. J. Tobin, Y. Okada, S. A. Ajuria, V. Lakhotia, W. A. Feil, and R. I. Hedge, J. Appl. Phys. **75**, 1811 (1994).
[6] C. M. M. Denisse, K. Z. Troost, J. B. Oude Elferink, F. H. P. M. Habraken, W. F. van der Weg, and M. Hendriks, J. Appl. Phys. **60**, 2536 (1986).
[7] C. Ance, F. d. Chelle, J. P. Ferraton, G. Leveque, P. Ordejon, and F. Yndurain, Appl. Phys. Lett. **60**, 1399 (1992).
[8] J. T. Yount, G. T. Kraus, P. M. Lenahan, and D. T. Krick, J. Appl. Phys. **70**, 4969 (1991).
[9] K. S. Seol, A. Ieki, Y. Ohki, H. Nishikawa, and M. Tachimori, J. Appl. Phys. **79**, 412 (1996).
[10] H. Nishikawa, E. Watanabe, D. Ito, and Y. Ohki, Phys. Rev. Lett. **72**, 2101 (1994).
[11] H. Nishikawa, E. Watanabe, D. Ito, M. Takiyama, A. Ieki, and Y. Ohki, J. Appl. Phys. **78**, 842 (1995).
[12] K. S. Seol, T. Futami, T. Watanabe, Y. Ohki, and M. Takiyama, J. Appl. Phys. **85**, 6746 (1999).
[13] K. S. Seol, T. Watanabe, M. Fujimaki, H. Kato, Y. Ohki, and M. Takiyama, Phys. Rev. B **62**, 1532 (2000).
[14] T. Noma, K. S. Seol, M. Fujimaki, H. Kato, T. Watanabe, and Y. Ohki, Jpn. J. Appl. Phys., Part 1 **39**, 6587 (2000).
[15] S. I. Raider, R. Flitsch, J. A. Aboaf, and W. A. Pliskin, J. Electrochem. Soc. **123**, 560 (1976).
[16] G. Lucovsky and S. Y. Lin, J. Vac. Sci. Technol. B **3**, 1122 (1985).

JOURNAL OF APPLIED PHYSICS VOLUME 91, NUMBER 10 15 MAY 2002

Photo-induced refractive index change in hydrogenated amorphous silicon oxynitride

Hiromitsu Kato[a)]
Department of Electrical, Electronics, and Computer Engineering, Waseda University, Shinjuku-ku 169-8555, Japan

Makoto Fujimaki
Advanced Research Institute for Science and Engineering, Waseda University, Shinjuku-ku 169-8555, Japan, Japan Science and Technology Corporation, Kawaguchi-shi 332-0012, Japan, and National Institute of Advanced Industrial Science and Technology, Tsukuba-shi 305-8568, Japan

Takashi Noma
Advanced Research Institute for Science and Engineering, Waseda University, Shinjuku-ku 169-8555, Japan and Engineering Department 1, System-LSI Division, Sanyo Electric Co. Ltd., Oizumi-Machi 370-0596, Japan

Yoshimichi Ohki
Department of Electrical, Electronics, and Computer Engineering, Waseda University, Shinjuku-ku 169-8555, Japan and Advanced Research Institute for Science and Engineering, Waseda University, Shinjuku-ku 169-8555, Japan

(Received 16 October 2001; accepted for publication 23 January 2002)

Refractive index change is shown to be induced by the irradiation of ultraviolet photons in hydrogenated amorphous silicon oxynitride films prepared by plasma-enhanced chemical vapor deposition. The mechanism of the index change and its dependence on the nitrogen content were investigated by electron spin resonance and scanning electron microscopy. It is concluded that the index change is due mainly to densification, and that the contribution of the formation of paramagnetic defects is only slight. To demonstrate the versatility of this refractive index change, a planar diffraction grating was fabricated. © *2002 American Institute of Physics.*
[DOI: 10.1063/1.1461894]

I. INTRODUCTION

The importance of hydrogenated amorphous silicon oxynitride (a-SiO_xN_y:H) films fabricated by plasma-enhanced chemical vapor deposition (PECVD) is increasing for low-cost highly integrated optical devices,[1–8] since the refractive index of a-SiO_xN_y:H is changeable over a wide range from 1.45, the value of silicon dioxide, to 2.00, that of silicon nitride, and since this allows considerable freedom in designing the structure of integrated optical devices.[9,10] Because the material is a compound of silicon, it is easily incorporated in the present fiber optic and large scale integrated circuit technologies. Moreover, as a PECVD-synthesized film, it has many advantages such as a low deposition temperature, large deposition area, ease of composition control, and excellent step coverage.[11–13]

Several papers have been reported on the effects of elementary composition or thermal annealing on the refractive index of a-SiO_xN_y:H.[3–6] However, to the authors' knowledge, no papers have reported on the refractive index change induced by UV photon irradiation, which potentially promises direct drawing of a waveguide[14] and direct fabrication of a waveguide with a buried periodic refractive index that can be used as an optical grating.[15] The present paper describes experimental measurements of the refractive index change induced in a-SiO_xN_y:H films by UV photon irradiation and discusses its mechanism. Moreover, a diffraction grating was fabricated using a phase lattice method to demonstrate the versatility of a-SiO_xN_y:H as a material for optical devices.

II. EXPERIMENTAL PROCEDURES

The a-SiO_xN_y:H films were deposited using a dual-frequency PECVD system. A mixture of SiH_4, N_2O, and N_2 gases was excited in a parallel-plate reactor where a RF power of 13.56 MHz was applied with a maximum power of 0.54 kW. At the same time, to reduce the structural stress, a low-frequency power of 400 kHz was also applied with a maximum power of 0.38 kW. Five types of films with different nitrogen contents were prepared by changing the flow rate of SiH_4, while the total pressure was kept constant around 2.4×10^2 Pa. The films were deposited onto a p-type silicon monocrystal wafer (100) set on a stage whose temperature was kept at 400 °C.

The elementary compositions of Si, O, and N were estimated through x-ray photoelectron spectroscopy (XPS JEOL-90MX). The refractive index and the thickness were measured by ellipsometry (Ulvac ESM-1) at a wavelength of 632.8 nm. Note that the accuracy of measurements is ± 0.005 for refractive index and ± 0.3 nm for thickness. A KrF excimer laser (wavelength: 248 nm=5.0 eV; pulse width: ~25 ns, Lambda Physik Compex 205) was used as the UV irra-

[a)]Research Fellow of the Japan Society for the Promotion of Science; electronic mail: 600c5050@nm.waseda.ac.jp

 © 2002 American Institute of Physics

TABLE I. Gas flow rates, elemental composition, and thickness of a-SiO_xN_y:H films studied.

Sample	Gas flow rate (sccm)			Composition at. %			Thickness (nm)
	SiH_4	N_2O	N_2	Si	O	N	
A	1.5×10^2	9.4×10^3	5.4×10^3	35	62	3.6	117.3
B	2.5×10^2	9.4×10^3	5.4×10^3	35	59	6.0	117.3
C	3.5×10^2	9.4×10^3	5.4×10^3	35	57	7.0	117.4
D	4.5×10^2	9.4×10^3	5.4×10^3	37	56	7.7	111.9
E	5.5×10^2	9.4×10^3	5.4×10^3	38	53	9.6	112.3

diation source. The electron spin resonance (ESR) spectra were obtained by JEOL JES-FA 300 at the *X*-band frequency. The density of paramagnetic centers was evaluated by double numerical integration of first-derivative spectra and comparison with the signal from diphenylpicrylhydrazyl ($g=2.0036$) of a known weight. The accuracy of the standard is believed to be ±20%. All the measurements were done at room temperature.

III. RESULTS

Table I shows the gas flow rates, elemental composition, and thicknesses of the a-SiO_xN_y:H films studied. With an increase in the flow rate of SiH_4, the nitrogen content increases and the oxygen content decreases, while the atomic composition deviates from the stoichiometric ratio. The degree of deviation of the atomic composition from the stoichiometric ratio can be judged by the stoichiometric factor expressed by $(1/2)x+(3/4)y$, which becomes unity if the sample is stoichiometric. Figure 1 shows the stoichiometric factor and the refractive index of each sample.

Figures 2(a), (b), and (c) show the changes in the refractive index (Δn) and that of the thickness in samples C, D, and E, respectively, induced by the irradiation of photons, with an energy density of 300 mJ/cm^2 per pulse and a pulse frequency of 10 Hz, from the KrF excimer laser. For samples A and B in which the nitrogen content is less than 6.0 at. %, it was not possible to measure Δn by ellipsometry at least up to the irradiation of 2.5×10^5 pulses. The induced refractive index Δn obtained for sample C is $\sim+1.5\times10^{-2}$ with the irradiation of 2.5×10^5 pulses [shown in Fig. 2(a)], and the one for D is $\sim+4.3\times10^{-2}$ with the irradiation of 1.5×10^4 pulses [Fig. 2(b)], while the one for E is $\sim+6.2\times10^{-2}$ with the irradiation of 1.8×10^3 pulses [Fig. 2(c)]. At the same time, the thickness decreases by 2.5, 5.3, and 5.6 nm in samples C, D, and E, respectively.

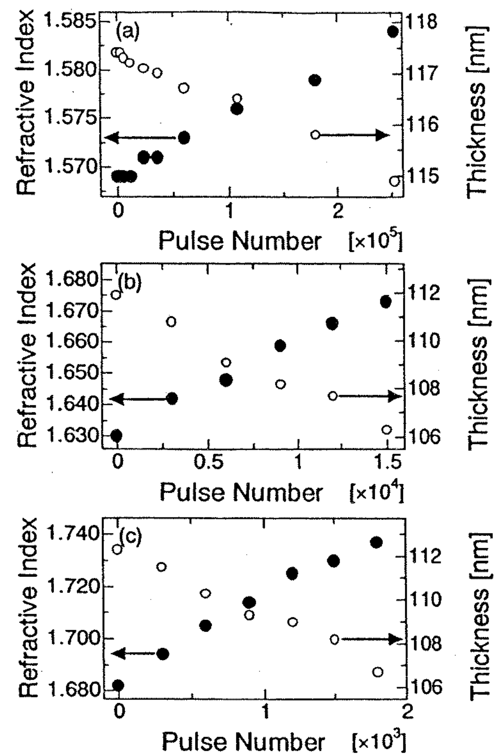

FIG. 2. Changes in the refractive index and the thickness in samples C (a), D (b), and E (c), induced by irradiation of photons from the KrF excimer laser. The solid and open circles indicate the refractive index and the thickness, respectively.

Figure 3 shows the average index change induced by one pulse of the KrF excimer laser, Δn/ pulse, as a function of the nitrogen content. As the nitrogen content increases, the value of Δn/pulse increases abruptly from 6.0×10^{-8} observed in sample C to 3.4×10^{-5} in sample E. This result clearly indicates that the UV sensitivity of a-SiO_xN_y:H becomes higher with a larger nitrogen content.

The ESR measurements were carried out for the samples irradiated by photons under the same conditions. Figures 4 and 5 show the ESR spectra and the densities of paramagnetic centers induced by the photon irradiation, respectively. Note that the spectra shown in Fig. 4 are those obtained after the photon irradiation of the aforementioned numbers of pulses, i.e., 2.5×10^5, 1.5×10^4, and 1.8×10^3 pulses for

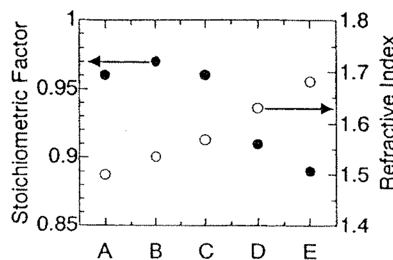

FIG. 1. The refractive index and stoichiometric factor of each sample. Letters below the abscissa are the sample names. The solid and open circles indicate the stoichiometric factor and refractive index, respectively.

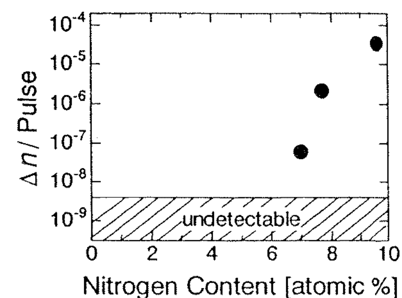

FIG. 3. Relation between the average refractive index change induced by one pulse of the KrF excimer laser and the nitrogen content.

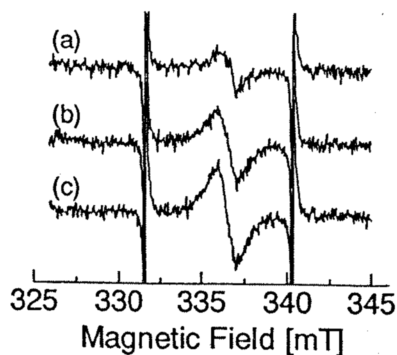

FIG. 4. The ESR spectra obtained for samples C (a), D (b), and E (c), induced by the photon irradiation of the KrF excimer laser.

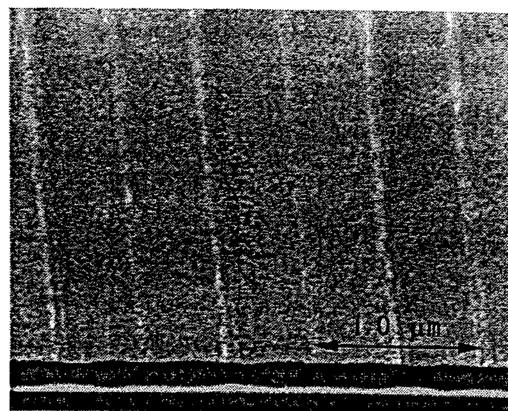

FIG. 6. A SEM image of the surface of a diffraction grating fabricated by the photon irradiation through a phase mask. A square-toothed pattern with periodicity of around 1 μm is seen. Each pattern consists of two bands with a nearly similar width of 0.5 μm. They are slightly different in color, and the darker one is a dented region densified by the irradiation.

samples C, D, and E, respectively, and that the densities shown in Fig. 5 are the averaged densities of paramagnetic defects induced by one pulse. The induced paramagnetic centers are attributable to silicon dangling bonds (Si–DBs).

Fabrication of a diffraction grating was performed on sample D using a phase mask made of a high quality fused silica plate transparent to the KrF excimer laser. The phase mask has a one-dimensional periodic surface-relief structure with a square-shaped cross section. The photons to fabricate the grating are from the KrF excimer laser and their energy density, pulse frequency, and the irradiation time were 640 mJ/cm^2 per pulse, 10 Hz, and 1 h, respectively. Figure 6 shows the surface of the grating observed by a scanning electron microscopy (SEM). A clear square-toothed pattern with periodicity of around 1 μm can be observed. Furthermore, a Fraunhofer diffraction pattern was successfully observed when a He–Ne laser beam was injected to the surface of this diffraction grating with an incidence angle of 75°. The periodicity of the square-toothed pattern on the grating can be estimated from the Fraunhofer diffraction pattern using the equation, $\sin \phi = -\sin \theta + m\lambda/d$, where λ is the wavelength, d the periodicity of the square pattern, θ the incidence angle, ϕ the diffraction angle, and m the order of diffraction. The estimated periodicity is around 1 μm, which agrees with the SEM image. This simply demonstrates that the present a-SiO_xN_y:H can be processed by UV photon irradiation.

IV. DISCUSSION

The induced refractive index change shown in Fig. 2 is large enough to fabricate waveguides or gratings.[1,5,8,16] Moreover, as shown in Fig. 3, the photosensitivity of a-SiO_xN_y:H can be easily controlled by the nitrogen content. To search for the best fabrication condition, the generation mechanism of the index change should be clarified. It is well known that there are two origins of the index increase, i.e., the densification of the material[14,17–20] and the paramagnetic defects.[21–24] As shown in Fig. 2, the thickness decreases in a manner opposite to the refractive index, indicating that the films are densified by the photon irradiation. The effect of densification on the index change was estimated using the Lorentz–Lorenz equation,[25,26] by assuming that the compaction occurred only in the direction of the thickness, since the estimation of the compaction in the surface direction was impossible. The contribution of the densification to the induced index change turns out to be 98%, 87%, and 70% for samples C, D, and E, respectively, as shown in Fig. 7. The densification obviously plays a major role in the increase of the refractive index.

Next, the effect of paramagnetic defects is discussed. The refractive index change due to the absorption increase can be in principle estimated using the Kramers–Kronig relation.[21] However, it is virtually impossible to obtain the sample's absorption spectrum in the UV region due to strong absorption by the silicon substrate. Therefore, we tried to use the following Smakula formula,[27]

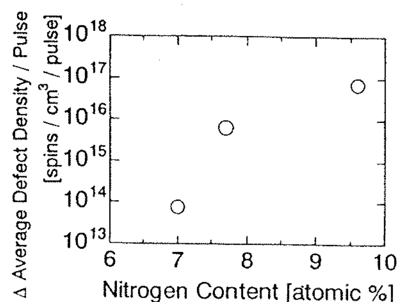

FIG. 5. Average density of paramagnetic defects induced by one pulse of the KrF excimer laser.

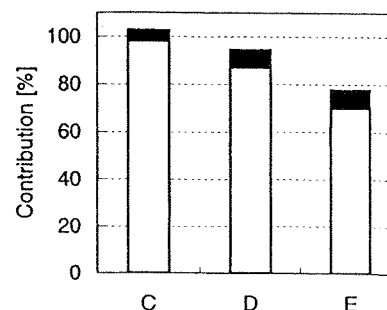

FIG. 7. Comparison of the contribution to the photo-induced refractive index increase between the densification (open bars) and the absorption due to paramagnetic centers (solid bars). Letters below the abscissa are the sample names.

$$Nf = 0.87 n \alpha \omega / (n^2+2)^2,$$

where n is the refractive index, α the absorption coefficient in cm^{-1} at the peak of the absorption band, ω the full width at half maximum (FWHM) in eV, N the defect density in cm^{-3}, and f the oscillator strength. As mentioned above, it is impossible to estimate the FWHM of the absorption due to the paramagnetic defects. The observed paramagnetic defects shown in Fig. 4 are solely Si–DBs. As a typical Si–DB, the E' center that has an absorption band at 5.8 eV is well-known. If these Si–DBs are assumed to be E' centers, the absorption coefficient induced in each sample by the paramagnetic defects can be calculated, since the oscillator strength and FWHM of the absorption at 5.8 eV are known.[28] The value of refractive index change induced by the paramagnetic defects can then be calculated using the Kramers–Kronig relation. The contribution of the paramagnetic defects to the index change was thus estimated to be 4.3% for sample C, 7.4% for sample D, and 7.7% for sample E, as shown in Fig. 7. The induced defects do not play a significant role in the increase of the refractive index. The fact that the sum of the two contributions is not equal to 100% is likely to be simply due to the inaccuracies of the ellipsometry and ESR measurements.

V. CONCLUSION

The photo-induced refractive index change in hydrogenated amorphous silicon oxynitride films with different nitrogen contents prepared by plasma-enhanced chemical vapor deposition was investigated. The index change induced by one pulse of the KrF excimer laser increases abruptly as the nitrogen content increases from 7.0 to 9.6 at. %, whereas the observable index change is not induced in the films with nitrogen contents less than 6.0 at. %. It is confirmed that the photorefractivity is due mainly to the densification, and that the role of the induced defects is small. It is also demonstrated that the photorefractivity can be utilized for the fabrication of optical gratings.

ACKNOWLEDGMENTS

This work was partly supported by Grants-in-Aid from Japan Society for the Promotion of Science for its Fellows (No. 1205733) and for Scientific Research (B) (No. 12450132). A High-Tech Research Grant from the Ministry of Education, Culture, Sports, Science, and Technology of Japan is also appreciated.

[1] B. Schauwecker, G. Przyrembel, B. Kuhlow, and C. Radehaus, IEEE Photonics Technol. Lett. **12**, 1645 (2000).
[2] K. B. Mogensen, P. Friis, J. Hubner, N. Petersen, A. M. Jorgensen, P. Telleman, and J. P. Kutter, Opt. Lett. **26**, 716 (2001).
[3] C. G. H. Roeloffzen, F. Horst, B. J. Offrein, R. Germann, G. L. Bona, H. W. M. Salemink, and R. M. de Ridder, IEEE Photonics Technol. Lett. **12**, 1201 (2000).
[4] R. M. de Ridder, K. Worhoff, A. Driessen, P. V. Lambeck, and H. Albers, IEEE J. Sel. Top. Quantum Electron. **4**, 930 (1998).
[5] M. Hoffmann, P. Kopka, and E. Voges, IEEE Photonics Technol. Lett. **9**, 1238 (1997).
[6] K. Worhoff, A. Driessen, P. V. Lambeck, L. T. H. Hilderink, P. W. C. Linders, and Th. J. A. Popma, Sens. Actuators A **74**, 9 (1999).
[7] B. S. Sahu, O. P. Agnihotri, S. C. Jain, R. Mertens, and I. Kato, Semicond. Sci. Technol. **15**, L11 (2000).
[8] T. S. Larsen, O. Leistiko, J. Electrochem. Soc. **144**, 1505 (1997).
[9] E. M. Dianov, K. M. Golant, R. R. Khrapko, A. S. Kurkov, and A. L. Tomashuk, J. Lightwave Technol. **13**, 1471 (1995).
[10] W. Gleine and J. Muller, Appl. Opt. **31**, 2036 (1992).
[11] C. P. Chang, C. S. Pai, and J. J. Hsieh, J. Appl. Phys. **67**, 2119 (1990).
[12] W. Kulisch, T. Lippmann, and R. Kassing, Thin Solid Films **174**, 57 (1989).
[13] C. S. Pai and C. P. Chang, J. Appl. Phys. **68**, 793 (1990).
[14] G. D. Maxwell and B. J. Ainslie, Electron. Lett. **31**, 95 (1995).
[15] M. V. Bazylenko, M. Gross, and D. Moss, J. Appl. Phys. **81**, 7497 (1997).
[16] B. Poumellec, P. Niay, M. Douay, and J. F. Bayon, J. Phys. D **29**, 1842 (1996).
[17] J. Heibei and E. Voges, Phys. Status Solidi A **57**, 609 (1980).
[18] J. Albert, B. Malo, K. O. Hill, D. C. Johnson, J. L. Brebner, and R. Leonelli, Opt. Lett. **17**, 1652 (1992).
[19] G. W. Arnold, J. Non-Cryst. Solids **179**, 288 (1994).
[20] M. Fujimaki, Y. Nishihara, Y. Ohki, J. L. Brebner, and S. Roorda, J. Appl. Phys. **88**, 5534 (2000).
[21] A. Anedda, C. M. Carbonaro, A. Serpi, N. Chiodini, A. Paleari, R. Scotti, G. Spinolo, G. Brambilla, and V. Pruneri, J. Non-Cryst. Solids **280**, 287 (2001).
[22] M. Fujimaki, T. Watanabe, T. Katoh, T. Kasahara, N. Miyazaki, Y. Ohki, and H. Nishikawa, Phys. Rev. B **57**, 3920 (1998).
[23] M. Fujimaki, T. Kasahara, S. Shimoto, N. Miyazaki, S. Tokuhiro, K. S. Seol, and Y. Ohki, Phys. Rev. B **60**, 4682 (1999).
[24] M. Fujimaki, T. Katoh, T. Kasahara, N. Miyazaki, and Y. Ohki, J. Phys.: Condens. Matter **11**, 2589 (1999).
[25] T. A. Dellin, D. A. Tichenor, and E. H. Barsis, J. Appl. Phys. **48**, 1131 (1977).
[26] V. V. Tugushev and K. M. Golant, J. Non-Cryst. Solids **241**, 166 (1998).
[27] A. Smakula, Z. Phys. **59**, 603 (1930).
[28] L. Skuja, J. Non-Cryst. Solids **239**, 16 (1998).

ELSEVIER

Nuclear Instruments and Methods in Physics Research B 191 (2002) 371–374

NIM B
Beam Interactions with Materials & Atoms

www.elsevier.com/locate/nimb

Evaluation of silica glasses implanted by high-energy ions using a UV-excited microspectroscopy

T. Yamaguchi [a], E. Watanabe [a], T. Souno [b], H. Nishikawa [b,*], M. Hattori [c], Y. Ohki [c], T. Kamiya [d], K. Arakawa [d]

[a] *Tokyo Metropolitan University, 1-1 Minami-Osawa, Hachioji-shi, Tokyo 192-0397, Japan*
[b] *Department of Electrical Engineering, Shibaura Institute of Technology, 3-9-14 Shibaura, Minato-ku, Tokyo 108-8548, Japan*
[c] *Waseda University, 3-4-1 Ohkubo, Shinjuku-ku, Tokyo 169-8555, Japan*
[d] *Japan Atomic Energy Research Insititute, Takasaki, 1233 Watanuki-machi, Takasaki-shi, Gunma 370-1292, Japan*

Abstract

In this study, defects induced by ion implantation were investigated by a photoluminescence (PL) microspectroscopy. When H^+ or He^{2+} with high energy (∼MeV) were implanted into silica, two PL bands at 290 and 650 nm were observed under 244 nm excitation. The PL bands at 290 and 650 nm were ascribed to oxygen deficient centers and nonbridging oxygen hole centers, respectively. The PL depth profile analysis shows that these PL centers are distributed throughout the tracks of ions, while they are quenched in the proximity of their projected ranges. Based on the observation on the PL profiles, the formation of the PL centers was ascribed to the energy deposition by electronic stopping power. The role of nuclear stopping power on the defect formation is also discussed. © 2002 Elsevier Science B.V. All rights reserved.

Keywords: Silica glass; Ion implantation; Photoluminescence; Microspectroscopy

1. Introduction

Silica glass is an important material widely used in advanced technology fields such as optical fibers and planar waveguides. Structural changes by ion implantation include defect formations by electronic excitation along the track of ions, [1] and refractive index changes at the projected ranges, R_p of ions associated with densification. [2] The ion implantation is a choice of technique for the fabrication of optical elements on planar waveguides, since it can provide the capability to control the R_p of ions. [3] The objective of this research is to evaluate the distribution in radiation effects on silica glass induced by MeV order implantation. In this study, we performed a photoluminescence (PL) mapping by a confocal microspectrometer equipped with a 244 nm laser. The distribution of the micron order gives new insights into the radiation effects in silica by MeV-order ion implantation.

2. Experimental procedures

Substrates for ion implantation are high-purity silica with different OH contents (EDC ([OH]< 1 ppm) and ES ([OH]:1200 ppm)). Protons or He^{2+}

* Corresponding author. Tel.: +81-3-5476-2456; fax: +81-3-5476-3068.
E-mail address: nishi@sic.shibaura-it.ac.jp (H. Nishikawa).

0168-583X/02/$ - see front matter © 2002 Elsevier Science B.V. All rights reserved.
PII: S0168-583X(02)00540-2

were implanted at 1–5 MeV up to doses of $0.5–5 \times 10^{15}$ cm^{-2}. Micro PL measurements were performed using a spectrometer (JASCO, NS2100NK) equipped with a confocal microscope. A frequency-doubled Ar laser of 244 nm was used as an excitation light source. For comparison, visible excitation at 514.5 or 488 nm was also used. Spatial resolution is axially ∼1.5 or 10 μm, and laterally is ∼1 μm.

3. Results and discussion

Shown in Fig. 1 are the PL spectra of H^+ and He^{2+} implanted silica observed under excitation at 488 nm. The PL spectra exhibit a PL band at 650 nm which is ascribed to the NBOHC (≡Si–O•, The symbols "≡" and "•" represent bondings with three separate oxygens and an unpaired spin, respectively) [4]. A PL band at 540 nm was observed in He^{2+} irradiated samples. The intensity of the 650 nm band *increases* with *decreasing* OH content. This indicates that the formation of NBOHCs can be due to the intrinsic mechanism from the normal Si–O–Si bond: [1]

$$\equiv\text{Si—O—Si}\equiv \rightarrow \equiv\text{Si—O}^\bullet + {}^\bullet\text{Si}\equiv, \quad (1)$$

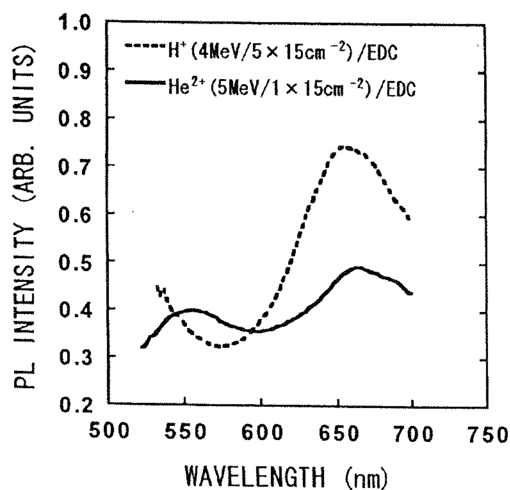

Fig. 1. The PL spectra of H^+ (4 MeV, 5×10^{15} cm^{-2}) and He^{2+} (5 MeV, 1×10^{15} cm^{-2}) implanted silica at room temperature for low-OH sample EDC ([OH] < 1 ppm) under 488 nm excitation.

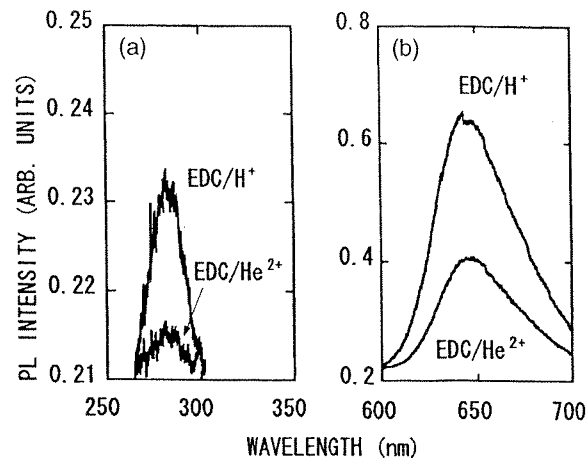

Fig. 2. PL spectra of H^+ (4 MeV, 5×10^{15} cm^{-2}) and He^{2+} (5 MeV, 1×10^{15} cm^{-2}) implanted silica (room temperature, 244 nm excitation) for low-OH sample EDC([OH]<1 ppm) and high-OH sample ES([OH]:1200 ppm) in ultraviolet (a) and visible (b) regions.

rather than the extrinsic mechanism associated with the fission of Si—OH bonds: [5]

$$\equiv\text{Si—OH} \rightarrow \equiv\text{Si—O}^\bullet + {}^\bullet\text{H}. \quad (2)$$

Shown in Fig. 2(a) and (b) are PL spectra of H^+ and He^{2+} implanted silica observed at room temperature under excitation at 244 nm. In addition to the 650 nm band, another PL band is observed at 290 nm. The 290 nm PL band is ascribed to oxygen-deficient centers II (ODCs II, ≡Si–Si≡), associated with the emission under excitation at $B_2\alpha$ band at 5.0 eV. [6] The 290 and 650 nm PL bands before and after implantation are compared in Fig. 3. The intensity of the 290 nm band for low-OH sample EDC ([OH] < 1ppm) is larger than that for high-OH sample ES ([OH]: 1200 ppm). Similar trends are observed for the 650 nm band due to NBOHCs. The 290 nm band observed for the low-OH sample EDC even before implantation is due to ODCs II introduced during the manufacture. The ODCs II and NBOHCs were less induced in silica with higher OH content. Hydrogen-related species such as H_2, which are mobile and reactive in silica, may be involved for the defect generation in high-OH silica.

For further understanding of the formation mechanisms of these PL centers, the distributions

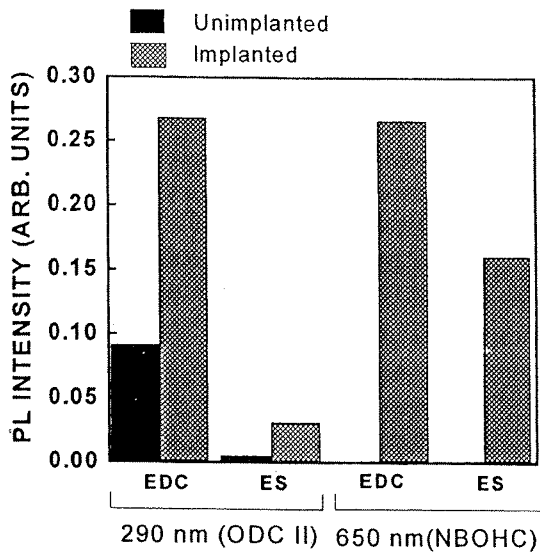

Fig. 3. Comparison of the PL intensities for unimplanted and H^+ implanted silica (low-OH sample EDC and high-OH sample ES, 4 MeV, 5×10^{15} cm^{-2}, room temperature, 244 or 514.5 nm excitation).

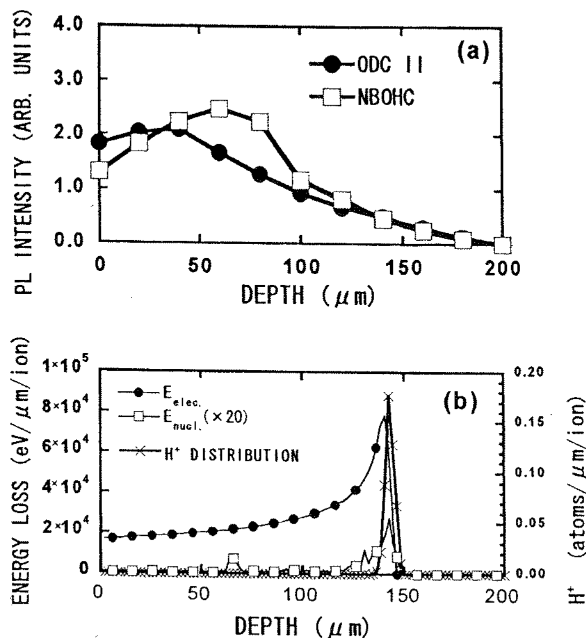

Fig. 4. Depth profiles of 290 nm band due to ODCs II for the low-OH (EDC) silica sample implanted by H^+ (4 MeV, 5×10^{15} cm^{-2}) obtained at room temperature, under 244 nm excitation (a) and calculated results of the energy losses due to electronic excitation and nuclear stopping using SRIM98 code (H^+, 4 MeV) (b).

of these ODCs and NBOHCs were investigated by mapping of their PL depth profiles for H^+-implanted silica, as shown in Fig. 4(a). The results of SRIM98 simulation [7] for the case of 4 MeV, H^+ implantation was performed and also shown in Fig. 4(b). The implanted 4-MeV H^+ ions lose most of their energies (99.99%) in silica by the electronic stopping power (E_{elec}), while the rest by nuclear stopping power (E_{nucl}). The profiles of E_{elec} and E_{nucl} show the maximum in the proximity of R_p. The E_{elec} also includes the energy loss from the surface to R_p of ~140 μm.

As shown in Fig. 4(a), the profiles of 290 and 650 nm bands show broad distributions with the maxima at 40 and 60 μm, respectively. Taking into account the energy loss profiles of Fig. 4(b), defect formations should be attributed to the E_{elec} whose contribution is much larger than the E_{nucl} in the region from the surface to the R_p, as previously reported. [1] We also note that the PL distributions of both ODCs II and NBOHCs do not perfectly agree with the distribution of E_{elec}. Similar trends were observed for He^{2+} implantation. It should be noted that the PL intensity diminishes at the forefront of the R_p or the maximum of the E_{nucl}, suggesting a possible role of the E_{nucl} in suppressing the formations of the ODCs II and NBOHCs. Also, we cannot rule out another possibility of the concentration quenching of PL, since the concentration of the PL centers is expected to be especially high in the proximity of the projected range where the electronic energy deposition also shows maximum as shown in Fig. 4(b).

Next, we discuss the formation mechanisms of the NBOHCs and ODCs II. Electronic excitation can result in both the generation of NBOHCs by Eq. (1) and ODCs II by the following reaction: [1]

$$\equiv\text{Si—O—Si}\equiv \;\rightarrow\; \equiv\text{Si—Si}\equiv + \text{O}_{\text{interstitial}}. \quad (3)$$

While the mechanism of Eq. (1) involving the breaking of Si—O—Si bond can be observed for a conventional electronic excitation such as a multiphoton excitation by UV lasers, the latter of Eq. (3) involves the Frenkel defect pair formations due to the dense electronic excitation, [1] which is inherent to the ion implantation.

4. Summary

Defect formation mechanisms in ion implanted silica were studied by means of depth-profile analysis using an UV-excited microspectroscopy. Since the energy loss due to E_{elec} is dominant in the region from the surface to projected ranges where the PL centers exist, the formation of ODC II and NBOHC can be ascribed to the energy deposition by E_{elec}. On the other hand, the formations of these defects are quenched in the proximity of the R_p, where the E_{nucl} is localized. This suggests the role of E_{nucl} in suppressing the formation of ODC II and NBOHC. In view of the future application of the MeV-order ion implantation to optical elements on silica glass, the information on the distribution of radiation effects gained by the UV-excited PL microspectroscopy is invaluable.

Acknowledgements

We acknowledge Dr. Fujimaki for providing the ion-implanted samples. This work is partly supported by Grants-in-Aid from Ministry of Education, Culture, Sports, Science and Technology, and by Iketani Foundation.

References

[1] H. Hosono et al., Phys. Rev. Lett. 80 (1998) 317.
[2] M. Fujimaki et al., J. Appl. Phys. 88 (2000) 5534.
[3] M. Fujimaki et al., Opt. Lett. 25 (2000) 88.
[4] L. Skuja, J. Non-Cryst. Solids 179 (1994) 51.
[5] H. Nishikawa, in: H.S. Nalwa (Ed.), Silicon-Based Materials and Devices, Vol. 2, Academic Press, New York, 2001, p. 93.
[6] H. Nishikawa et al., Phys. Rev. Lett. 72 (1994) 2101.
[7] J.F. Ziegler, J.P. Biersack, U. Littmark, The Stopping and Range of Ions in Solids, Pergamon Press, New York, 1985.

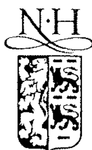

ELSEVIER

Nuclear Instruments and Methods in Physics Research B 191 (2002) 362–365

NIM B Beam Interactions with Materials & Atoms

www.elsevier.com/locate/nimb

Characterization of ion-implanted silica glass by vacuum ultraviolet absorption spectroscopy

M. Hattori [a], Y. Nishihara [a], Y. Ohki [a,*], M. Fujimaki [b], T. Souno [c], H. Nishikawa [c], T. Yamaguchi [d], E. Watanabe [d], M. Oikawa [e], T. Kamiya [e], K. Arakawa [e]

[a] *Department of Electrical, Electronics and Computer Engineering, Waseda University, 3-4-1 Ohkubo, Shinjuku-ku, Tokyo 169-8555, Japan*

[b] *JST, 4-1-8 Honmachi, Kawaguchi-shi, Saitamaken 332-0012, Japan*

[c] *Shibaura Institute of Technology, 3-9-14 Shibaura, Minato-ku, Tokyo 108-8548, Japan*

[d] *Tokyo Metropolitan University, 1-1 Minami-Osawa, Hachioji, Tokyo 192-0397, Japan*

[e] *JAERI Takasaki, 1233 Watanuki-machi, Takasaki, Gunma 370-1292, Japan*

Abstract

We investigate the mechanisms of defect formation and optical absorption induced by ion implantation, for fabrication of optical devices by radiation effects. High-purity silica implanted by H^+ or He^{2+} was characterized using vacuum-ultraviolet spectroscopy and electron-spin-resonance measurement. Defect formation is suppressed by OH groups, possibly by the release of atomic hydrogen. The E′ center and nonbridging oxygen hole center were created through pair generation from the normal Si—O—Si bond. The peroxy radical was generated through the reaction of the E′ center with interstitial oxygen, which is a Frenkel-defect pair with an oxygen vacancy. By the Kramers–Kronig analysis on the MeV-ion implantation-induced defects, a refractive index increase of the order of 10^{-4} was estimated. © 2002 Elsevier Science B.V. All rights reserved.

Keywords: Silica glass; Ion implantation; Vacuum ultraviolet; Electron spin resonance

1. Introduction

Fabrication of optical devices such as optical fiber gratings has been reported by our group using mega-electron-volt-order ion implantation on silica-core optical fibers [1]. In order to extend this technique for the fabrication of silica-based planar optical devices, it is important to understand the mechanisms by which changes in optical properties such as refractive index are induced by the implanted ions. Attention is focused on the electronic stopping energy loss, since it accounts for more than 99% of the total loss and most defects are induced through this process in the case of MeV-order ion implantation.

2. Experimental procedures

Samples are two types of high-purity silica glasses containing different OH contents, EDC (OH content <1 ppm) and ES (OH content = 1200 ppm). They are plates with an area of 100 mm^2 and a thickness of 1 mm, and were implanted with H^+ and He^{2+} ions accelerated to energies of 4 and 5 MeV,

* Correrspondng author. Fax: +81-3-3204-1258.
E-mail address: yohki@mn.waseda.ac.jp (Y. Ohki).

0168-583X/02/$ - see front matter © 2002 Elsevier Science B.V. All rights reserved.
PII: S0168-583X(02)00537-2

respectively. Ultraviolet (UV) and vacuum ultraviolet (VUV) absorption spectra were measured with spectrometers using synchrotron radiation as a VUV photon source. Electron-spin resonance (ESR) spectra were recorded at 77 K, while the microwave power was changed between 1 mW and 1 μW to separate overlapping components.

3. Results and discussion

The insets of Fig. 1 show the absorption spectra. Before ion implantation, the 7.6 eV absorption band due to oxygen-deficient-center (ODC) I [2] was observed only in the oxygen-deficient-type EDC. The absorbance increases by implantation of H^+ or He^{2+} ions by a smaller amount in ES containing OH groups of 1200 ppm, as previously observed for the case of γ-irradiation [3]. This suggests that atomic hydrogens released from the OH groups terminate the defects created by the bond cleavage induced by the electronic excitation [2,3]. The induced absorption spectra shown in Fig. 1 are fitted with five Gaussian absorption bands at 4.8, 5.02, 5.8, 7.15 and 7.6 eV, which are respectively ascribed to nonbridging oxygen hole center (NBOHC), ODC II, E′ center, an unknown defect, and ODC I [4,5]. Fig. 2 shows ESR spectra recorded with a microwave of power of 1 mW. Paramagnetic defects such as E′ center, NBOHC and peroxy radical (PR) are observed.

Fig. 3 shows the correlation between the concentration of E′ centers and that of NBOHCs induced by ion implantation estimated from the absorption spectra and ESR measurements. The defect concentration was estimated from the absorption spectra using the Smakula formula [6]. It was also estimated by doing double numerical integration of each spectrum after fitting the ESR spectrum with component spectra [7]. An almost one-to-one correlation between the E′ center and NBOHC is observed for both samples EDC and ES, which indicates that pair generation of the E′ center and NBOHC through the breaking of Si—O—Si bond:

$$\equiv\text{Si—O—Si}\equiv \rightarrow \equiv\text{Si}^\bullet\ {}^\bullet\text{O—Si}\equiv, \quad (1)$$

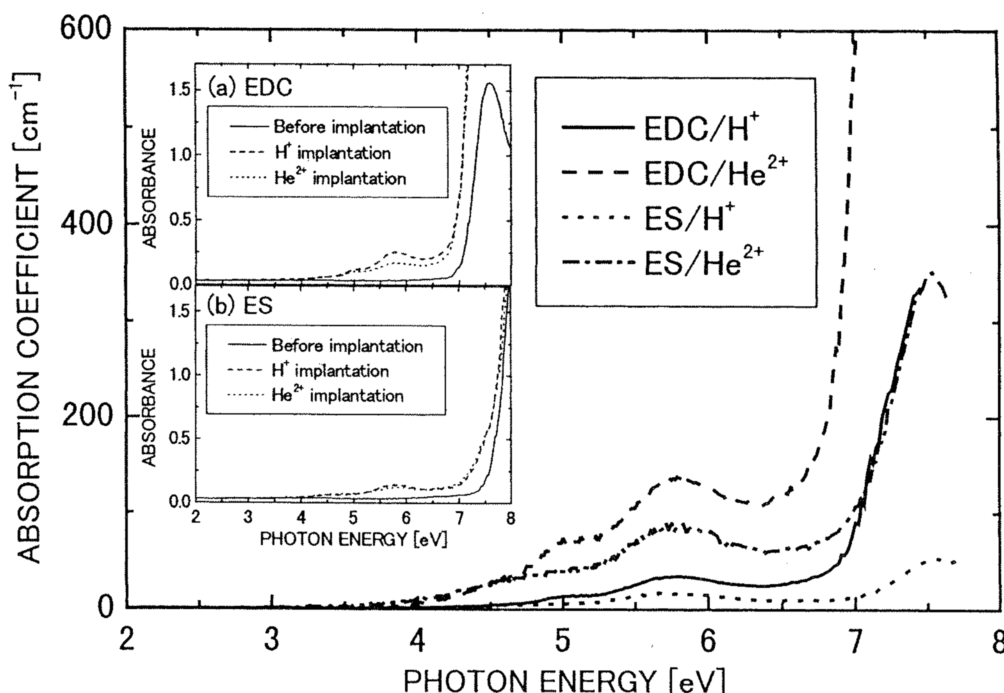

Fig. 1. Ion-implantation-induced absorption spectra in units of absorption coefficients given by dividing the absorbance spectra by the projected ranges 146 μm for H^+ and 23 μm for He^{2+} ions for EDC and ES. Shown in the inset of Fig. 1 are spectra in units of absorbance.

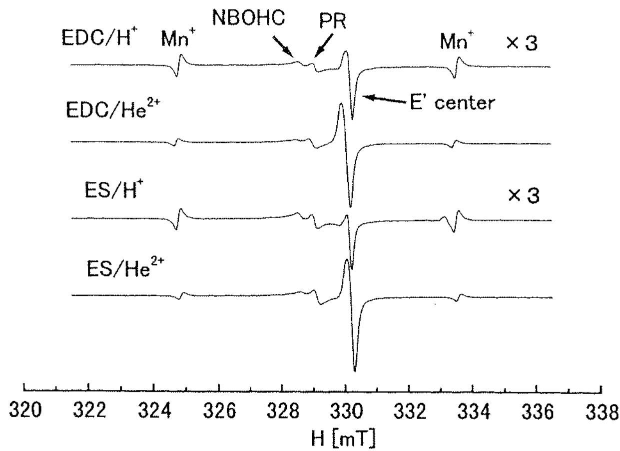

Fig. 2. ESR spectra observed after H^+ or He^{2+} implantation for EDC and ES at a microwave power of 1mW.

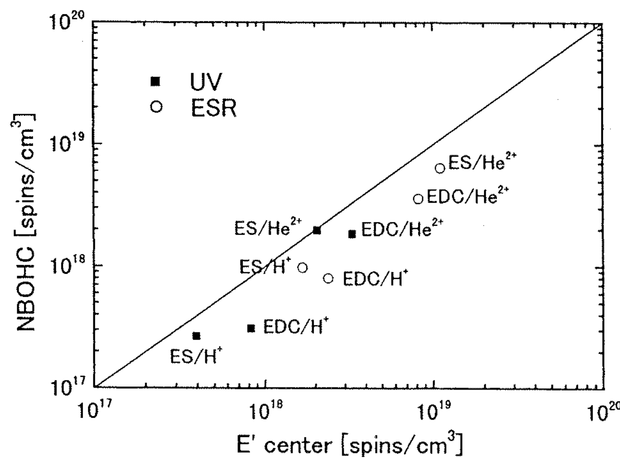

Fig. 3. Correlation between concentrations of E′ center and NBOHC induced by ion implantation. The solid squares and the open circles are estimated by the UV spectra and the ESR spectra, respectively.

where the symbol "•" denotes an unpaired electron.

This defect formation mechanism is the same as in the cases of excimer laser and γ-ray irradiation [3,8]. As shown in Fig. 4, the concentration of PRs is independent of the OH content, but is dependent on the ion implantation condition. In the case of the stoichiometric ES, the concentration of ODCs I is nearly comparable to that of PRs. It is reported that Frenkel defect formation and subsequent reactions are induced by electronic excitation [2,9]:

$$\equiv\text{Si—O—Si}\equiv \rightarrow \equiv\text{Si—Si}\equiv + \text{O}_{\text{int}}, \quad (2)$$

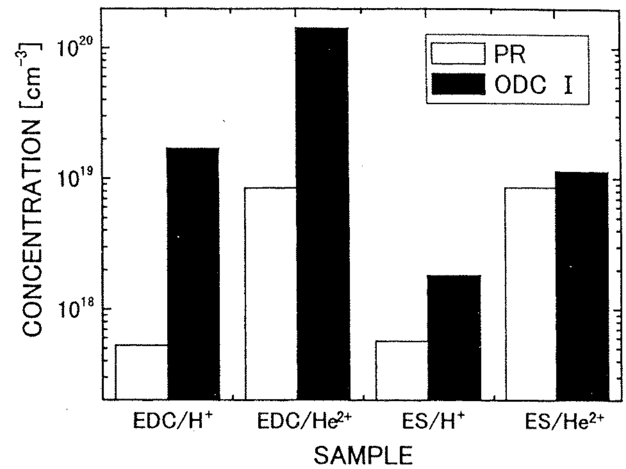

Fig. 4. PR and ODC I induced by ion implantation.

$$2\text{O}_{\text{int}} \rightarrow \text{O}_2, \quad (3)$$

$$\equiv\text{Si}^{\bullet} + \text{O}_2 \rightarrow \equiv\text{Si—O—O}^{\bullet}. \quad (4)$$

From reactions (2) to (4), the number of the induced PRs should be half of that of ODCs I. In the case of sample ES, there is a relatively good agreement as to those numbers, which suggests for ES that PRs and ODCs I are created as a result of reactions (2)–(4). As for the oxygen-deficient EDC, the ODCs I are over ten times as many as PRs. The 7.6 eV absorption band due to ODC I clearly appears before ion implantation, as shown in Fig. 1. The 5.02 eV band due to ODC II, the defect which is considered to be in thermal equilibrium with ODC I, appears only in EDC. This fact and the fact that the number of ODC I present in EDC is more than the one in ES suggest that the oxygen deficiency of EDC enhances the generation of the two types of ODCs. The refractive index change induced by the increase in absorption was estimated by the Kramers–Kronig relation and is approximately of the order of 10^{-4}, as shown in Table 1. This index change is considered to be induced from the surface to the projected range of

Table 1
Refractive index changes estimated by the Kramers–Kronig relation.

	EDC/H+	EDC/He2+	ES/H+	ES/He2+
Δn	1.19×10^{-4}	8.54×10^{-4}	2.37×10^{-5}	1.53×10^{-4}

ions, where the defects responsible for the UV and VUV absorption bands were induced by the electronic stopping power. It should be noted that a higher refractive index change of the order of 10^{-3} is induced, due to the nuclear stopping power in the region near the projected range [1].

4. Conclusion

The effects of electronic stopping energy loss in H^+ and He^{2+}-implanted silica glasses were studied by means of UV to VUV absorption spectroscopy and ESR. It was found that OH groups can suppress the defect generation. Pair generation of E′ centers and NBOHCs through the breaking of Si—O—Si bonds are suggested from the one-to-one correlation in their concentrations. It is also suggested for stoichiometric silica that PRs were created by the reaction of E′ centers with interstitial oxygens, which were generated as Frenkel-defect pairs with ODCs I. On the other hand, oxygen deficiency is considered to play a role in the enhanced generation of ODCs I and II. A refractive index change of the order of 10^{-4} is expected from these defects induced by the MeV-ion implantation.

References

[1] M. Fujimaki et al., J. Appl. Phys. 88 (10) (2000) 5534.
[2] H. Hosono et al., Nucl. Instr. and Meth. B 141 (1998) 566.
[3] Y. Kawaguchi et al., J. Appl. Phys. 80 (10) (1996) 5633.
[4] M. Verhaegen et al., Appl. Phys. Lett. 68 (1996) 3084.
[5] M. Antonini et al., Radiat. Eff. 65 (1982) 41.
[6] D.W. Cooke et al., J. Appl. Phys. 87 (11) (2000) 7793.
[7] D.L. Griscom et al., J. Non-Cryst. Solids 32 (1979) 313.
[8] H. Imai et al., J. Non-Cryst. Solids 179 (1994) 202.
[9] N. Matsunami et al., Phys. Rev. B 60 (1999) 10616.

ELSEVIER

Nuclear Instruments and Methods in Physics Research B 191 (2002) 342–345

NIM B
Beam Interactions with Materials & Atoms

www.elsevier.com/locate/nimb

Radiation effects and surface deformation of silica by ion microbeam

H. Nishikawa [a,*], T. Souno [a], M. Hattori [b], Y. Nishihara [b], Y. Ohki [b], E. Watanabe [c], M. Oikawa [d], T. Kamiya [d], K. Arakawa [d]

[a] *Shibaura Institute Technology, 3-9-14 Shibaura, Minato-ku, Tokyo 108-8548, Japan*
[b] *Waseda University, 3-4-1 Ohkubo, Shinjuku-ku, Tokyo 169-8555, Japan*
[c] *Tokyo Metropolitan University, 1-1 Minami Osawa, Hachioji, Tokyo 192-0397, Japan*
[d] *JAERI Takasaki, 1233 Watanuki-machi, Takasaki, Gunma 370-1292, Japan*

Abstract

Radiation effects induced by ion microbeam were studied by a confocal microspectroscopy and an atomic force microscopy (AFM). We investigate two significant radiation effects, defect generation and compaction, which were ascribed to electronic (E_{elec}) and nuclear stopping powers (E_{nucl}), respectively. Photoluminescence mapping of non-bridging oxygen hole centers at 650 nm reveals the defect formation along the tracks of ions. The surface deformation measured by AFM depends on the width of irradiated by microbeam. Confinement effects from the interface of irradiated and nonirradiated regions are taken into account for the understanding of the correlation between the surface deformations and internal compactions. © 2002 Elsevier Science B.V. All rights reserved.

Keywords: Silica; Ion microbeam; Photoluminescence; Atomic force microscopy

1. Introduction

Much attention has been paid to the radiation effects induced by high-energy particles and photons on silica over the past several decades, since they have capabilities in modifying the properties of silica-based optical elements [1]. In this study, radiation effects on silica by ion microbeam were investigated by means of a micro-PL (photoluminescence, PL) spectroscopy and atomic force microscopy (AFM). Correlation of surface deformation with radiation effects is also discussed.

2. Experimental procedures

Ions (H^+, He^+ or Si^{5+}) with energies in the range of 2–18 MeV were implanted into high-purity silica substrates with various OH contents (<1–1200 ppm) using a microbeam line (TIARA, JAERI Takasaki, beam diameter: ~1 μm). For comparison, silica glasses implanted with macrobeam of H^+ or He^{2+} at energies of 1–5 MeV were also studied. Micro-PL-Raman spectrometers equipped with an Ar ion laser (488, 514.5 or 244 nm (SHG)) were used for the mapping of

* Corresponding author. Fax: +81-3-5476-3068.
E-mail address: nishi@sic.shibaura-it.ac.jp (H. Nishikawa).

0168-583X/02/$ - see front matter © 2002 Elsevier Science B.V. All rights reserved.
PII: S0168-583X(02)00530-X

the PL. Topographic images of the silica surface were measured by AFM.

3. Results and discussion

Three PL bands at 290, 540 and 650 nm were observed for ion-implanted silica. Since the 650 nm PL due to nonbridging oxygen hole centers (NBOHCs) (≡Si–O·, the symbols "≡" and "·" represent bondings with three separate oxygens and an unpaired spin, respectively) [2] is relatively intense, we used the PL as a probe to visualize the radiation effects. Shown in Fig. 1 is a result of the 650-nm PL mapping for 3-μm-line width area by H^+ microbeam. The projected range R_p is estimated to be ~47 μm by SRIM98 [3] for the 2.2 MeV H^+ implantation with a 7.5-μm-thick polyimide film on the surface. The PL distribution can be seen in the regions up to the depth of ~40 μm, which is shallower than the R_p as shown in Fig. 1. It is therefore considered that the generation of NBOHCs is due to the energy loss by E_{elec} rather than that due to E_{nucl} as previously reported [4].

Despite the E_{elec} maximum at R_p from SRIM98 data, the PL intensity abruptly diminished around ~40 μm, which is shallower than the R_p of ~47 μm. Similar quenching phenomena were also observed for the 290-nm PL band associated with oxygen deficient centers (ODC, ≡Si–Si≡) for different conditions (H^+ or He^{2+}, 1–5 MeV). It is therefore suggested that the E_{nucl} suppresses the formation of these defects. Based on these observations, the E_{nucl} as well as the E_{elec}, should be taken into consideration to explain the radiation effect associated with defect generations.

Fig. 2 present the AFM image (a) and the profile (b) of the microbeam-irradiated silica (Si^{5+}, 18 MeV, dose: 1.0×10^{14} cm^{-2}). The surface image in Fig. 2(a) indicates the formation of grooves with depths of up to ~90 nm. The depth of the grooves

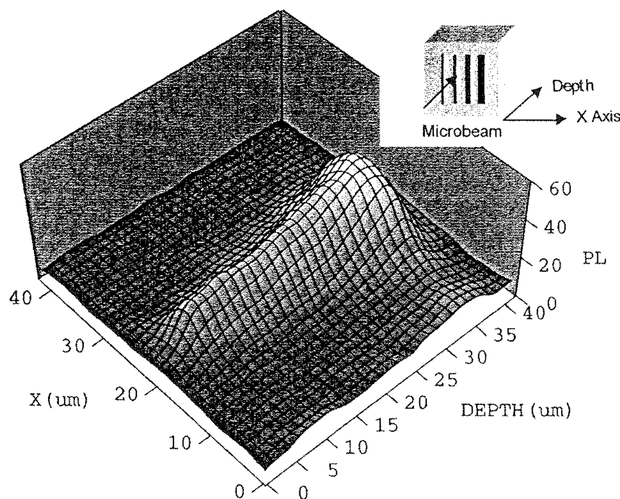

Fig. 1. Cross-sectional distribution of the PL intensity at 650 nm observed for a rectangular shaped region (3 μm × 350 μm) with microbeam (H^+, 2.2 MeV, dose: 1×10^{15} ions/cm^2).

(a)

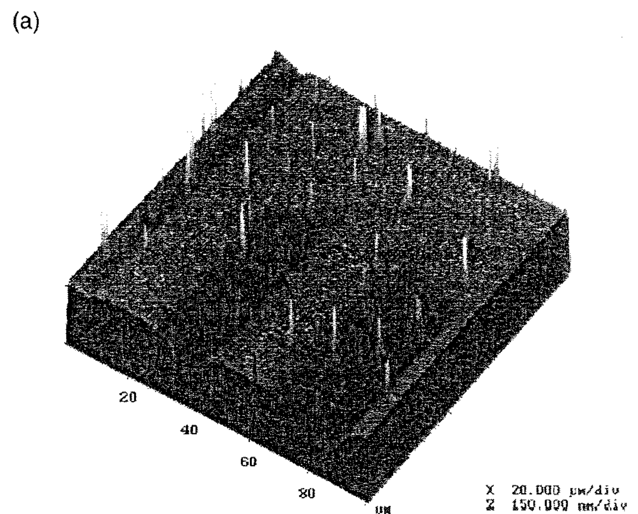

(b)

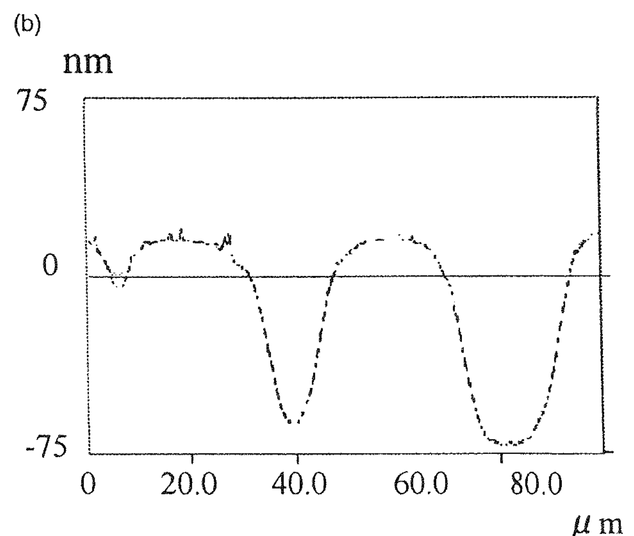

Fig. 2. (a) The AFM image and (b) the profile of the microbeam-irradiated regions (Si^{5+}, 18 MeV, dose: 1.0×10^{14} ions/cm^2).

depends on the ion species and the implanted areas. The width of the groove is larger than the irradiated area by a factor of 2–4, with the edges being round shaped as shown in Fig. 2(b). For mm-scale macrobeam irradiation on silica, the surface deformation is reported to be a result of internal compaction in the vicinity of R_p of ions, where the E_{nucl} is localized [5]. The same mechanism is expected to be in effect for the case of microbeam. However, the microbeam-induced deformation is dependent on the line width, while for the case of macrobeam it is determined by deposited energy by E_{nucl}. Then, what determines the surface deformation for microbeam? A major difference is the scale of the irradiated region. For μm-scale irradiation by microbeam, effects from the surrounding regions must be larger for a smaller line width, where effects such as confinements from both edges can modify the surface deformation.

We, hereafter, refer to the interface bordering the irradiated and nonirradiated regions as "radiation interface". For further investigation on the radiation interface, we carried out an AFM measurement across the radiation interface for macrobeam-irradiated silica, as shown in Fig. 3. Similar to the round-shaped edges of the grooves in Fig. 2, a slope across the interface can be seen in Fig. 3. The right hand plateau in Fig. 3 can be regarded as a state of full deformation, which reflects the internal compaction at the R_p. The radiation interface is now characterized as a transition region with μm-scale width, gradually relaxing toward a fully deformed state.

The PL mapping analysis on the macrobeam-irradiated silica was further carried out to characterize the radiation interface under the surface. Figs. 4(a) and (b) show a typical PL mapping image of the NBOHCs across the radiation interface for H^+-implanted silica with 2 MeV, and the schematic illustration of the radiation interface, respectively. The PL intensity shows a maximum at the radiation interface and a plateau in irradiated regions. Such a localization of intense PL maximum at the radiation interface suggests the enhanced generation of the NBOHCs by the interfacial stress. As illustrated in Fig. 4(b), the PL

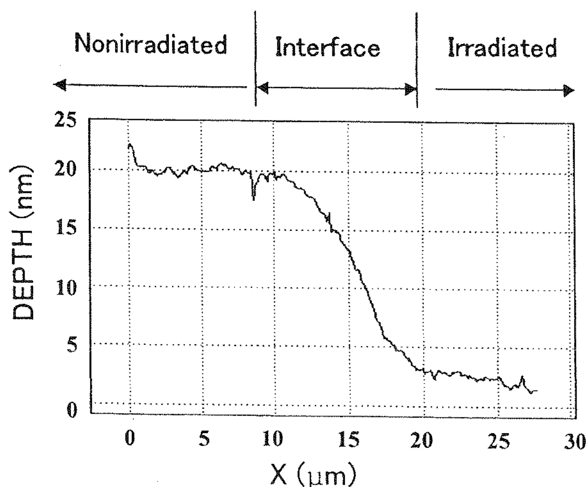

Fig. 3. Surface profile measured by AFM for macrobeam-irradiated silica (He^{2+}, 1 MeV, dose: 1×10^{15} ions/cm^2) at the border of nonirradiated/irradiated interface.

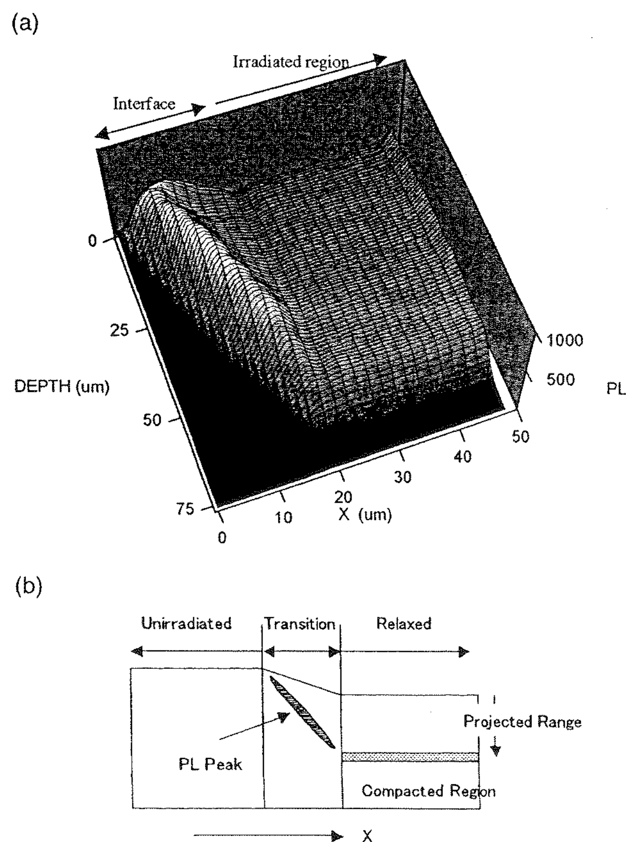

Fig. 4. The PL image at the border across the nonirradiated and irradiated regions observed for macrobeam-irradiated silica (H^+, 2 MeV, dose: 1×10^{15} ions/cm^2) (a), and the schematic illustration of the cross section including transition region of radiation interfaces (b).

maximum stretches from the surface to the R_p. The enhanced PL at the interface was also observed for other samples irradiated under different conditions.

The surface deformation by ion microbeam in Fig. 2 can be qualitatively understood in the following way. The grooves can be regarded as a region confined by the two radiation interfaces, where the stresses in opposite directions are exchanged. With increasing line width, the compressive stress from compacted regions at R_p will be developed, while the tensile stress from non-irradiated region stays constant. Therefore, the surface deformation is determined by the distribution and the degree of internal compaction, which determine the stress distribution at the radiation interface.

4. Summary

Radiation effects induced by ion microbeam were investigated by a PL microspectroscopy and AFM. The PL mapping is an effective method to visualize the three dimensional distribution of PL centers, which can be seen as an index of a radiation effect by E_{elec}. Surface deformation depends on the irradiated line width. This can be explained by the radiation interface between irradiated and nonirradiated regions, where the structure of silica is in transition from an unrelaxed to a fully relaxed state. The stresses in the opposite directions are exchanged at the radiation interface, thereby exercising a significant influence on the surface deformation of μm-scale line width.

Acknowledgements

We acknowledge Dr. Fujimaki for providing some of the ion-implanted samples. This work is partly supported by Grants-in-Aid from Ministry of Education, Culture, Sports, Science and Technology.

References

[1] H. Nishikawa, in: H.S. Nalwa (Ed.), Silicon-Based Materials and Devices, Vol. 2, Academic Press, 2001, p. 93.
[2] L. Skuja, J. Non-Cryst. Solids 239 (1998) 16.
[3] J. F. Ziegler et al., The Stopping and Range of Ions in Solids, Pergamon Press, New York, 1985.
[4] H. Hosono, H. Kawazoe, N. Matsunami, Phys. Rev. Lett. 80 (1998) 317.
[5] M. Fujimaki, Y. Nishihara, Y. Ohki, J.L. Brebner, S. Roorda, J. Appl. Phys. 88 (2000) 5534.

JOURNAL OF APPLIED PHYSICS VOLUME 93, NUMBER 1 1 JANUARY 2003

Band-tail photoluminescence in hydrogenated amorphous silicon oxynitride and silicon nitride films

Hiromitsu Kato,[a] Norihide Kashio, and Yoshimichi Ohki[b]
Department of Electrical, Electronics, and Computer Engineering, Waseda University, Shinjuku-ku 169-8555, Japan

Kwang Soo Seol[b]
RIKEN (The Institute of Physical and Chemical Research), Wako 351-0198, Japan

Takashi Noma[b]
Engineering Department 1, System-LSI Division, Sanyo Electric Co. Ltd., Oizumi-Machi 370-0596, Japan

(Received 7 August 2002; accepted 23 October 2002)

Photoluminescence (PL) measurements were performed on a series of hydrogenated amorphous silicon oxynitride and silicon nitride films with different nitrogen contents deposited by plasma-enhanced chemical-vapor deposition. From the PL and PL excitation spectra, the Urbach energy of the sample is found to be proportional to its PL half-maximum width, regardless of whether the sample is silicon oxynitride or silicon nitride. Time-resolved PL measurements showed that PL peak energy varies with time after the excitation, showing a systematic dependence on the chemical composition in the two materials. That the PLs observed in the two materials have very similar characteristics regardless of the presence of oxygen strongly indicates that the PLs result from the same chemical structure, more specifically Si–N bonds, and that the two materials have similar band-tail states associated with the static disorder. In the two materials, it is found that the electrons and holes photoexcited into such band-tail states recombine first through an excitonlike recombination process and then through a radiative tunneling recombination process. © *2003 American Institute of Physics.* [DOI: 10.1063/1.1529292]

I. INTRODUCTION

Hydrogenated amorphous silicon oxynitride ($a-SiO_xN_y$:H) and silicon nitride ($a-SiN_z$:H) have been receiving considerable attention not only as suitable isolators for electronic devices such as very-large-scale integrated circuits,[1–4] but also as optical materials for waveguides,[5,6] light emitting devices,[7] and solar cells.[8,9] With the rapid and continuing progress of technologies in electronics and photonics, the importance of these amorphous materials is continually increasing. Unfortunately, these films are known to contain many defects and localized states that deteriorate the device performance, especially when they are prepared by plasma-enhanced chemical-vapor deposition (PECVD). From this point of view, the authors have been studying the defects and structural disorder in the two materials by analyzing their photoluminescence (PL) properties.[10–15] We have shown that $a-SiO_xN_y$:H and $a-SiN_z$:H films exhibit a broad PL with a peak energy around 2.2–2.9 eV.[10–15] Although much work has been done for the PL in $a-SiN_z$:H,[14–18] little is known about the PL in $a-SiO_xN_y$:H. While we have indicated that the PL in $a-SiO_xN_y$:H is due to radiative recombination between localized band-tail states associated with Si–N bonds similar to $a-SiN_z$:H,[10–15] its detailed properties such as the decay process and the effect of chemical composition are unknown. In the present article, the band-tail PL around 2.2–2.9 eV in $a-SiO_xN_y$:H is examined by comparing its PL spectral shape, width of band-tail states, and PL lifetime distribution with those of the PL in $a-SiN_z$:H.

II. EXPERIMENTAL PROCEDURES

The $a-SiO_xN_y$:H films were deposited using a dual-frequency PECVD system. A mixture of SiH_4, N_2O, and N_2 gases was excited in a parallel-plate reactor where a rf power of 13.56 MHz was supplied with a maximum power of 0.54 kW. At the same time, a lower-frequency power of 400 kHz was also supplied with a maximum power of 0.38 kW to reduce the structural stress of the deposited film. Three types of films with different atomic ratios were prepared by changing the flow ratio of SiH_4 to the sum of the other two gases, while the total pressure was kept constant around 2.4×10^2 Pa. The films were deposited onto a *p*-type (100) silicon monocrystal substrate set on a stage whose temperature was kept constant at 400 °C. Three types of $a-SiN_z$:H films were similarly deposited using a mixture of SiH_4, N_2, and NH_3 gases. The elemental compositions of Si, O, and N were estimated through x-ray photoelectron spectroscopy (XPS, JEOL JPS-90MX). The refractive index was measured by ellipsometry (ULVAC ESM-1) at a wavelength of 632.8 nm with a He–Ne laser.

In order to obtain PL spectra, two photon sources were used. One is synchrotron radiation (SR) under multibunch operation at the BL1B line of UVSOR Facility (Institute for

[a] Research Fellow of the Japan Society for the Promotion of Science; electronic mail: hiromitsu_kato@asagi.waseda.jp
[b] Present address: Advanced Research Institute for Science and Engineering, Waseda University, Shinjuku-ku 169-8555, Japan.

0021-8979/2003/93(1)/239/6/$20.00 © 2003 American Institute of Physics

TABLE I. Elemental compositions, gas flow rates, abundance ratios of atoms other than silicon to silicon atoms, and refractive indices of $a-SiO_xN_y$:H, and $a-SiN_z$:H films.

Sample	Gas flow ratio	Atomic %			Abundance ratio	Refractive index
Silicon oxynitride	$SiH_4/(N_2O+N_2)$	Si	O	N	{(1/2)O+(3/4)N}/Si	
A	4.4×10^{-2}	39	51	9.7	0.84	1.74
B	3.7×10^{-2}	38	53	9.6	0.89	1.68
C	3.0×10^{-2}	37	56	7.7	0.91	1.63
Silicon nitride	$SiH_4/(NH_3+N_2)$	Si		N	{(3/4)N}/Si	
D	1.2×10^{-1}	52		47	0.68	2.08
E	8.6×10^{-2}	50		49	0.73	1.99
F	5.1×10^{-2}	44		55	0.95	1.91

Molecular Science, Okazaki, Japan) and the other is a KrF excimer laser (wavelength: 248 nm=5.0 eV, pulse width: ~25 ns, pulse energy: ~100 mJ/cm^2, Lambda Physik Compex 205). The spectra were measured using a monochromator equipped with an intensified charge-coupled device (ICCD) array. As for photoluminescence excitation (PLE) spectra, the SR photons under multibunch were used. The photon energy to be detected was fixed at the PL peak energy using an interference filter (transmittance: ~40%, full width at half maximum: ~15 nm) and the intensity of detected photons was monitored by a photomultiplier (Hamamatsu R955) as a function of the excitation SR photon energy.

Nanosecond-order PL decay characteristics were measured using the SR photons under single-bunch operation (time interval of SR pulses: 177.6 ns, apparent pulse width: 550 ps). The number of photons with energies around the PL peak through the interference filter was counted by a microchannel-plate photomultiplier (Hamamatsu R3809U-52) with a time-correlated single-photon counting technique. Time-resolved PL spectra were measured using the excimer laser and a monochromator equipped with an intensified charge-coupled device (ICCD) array. The ICCD array was gated by a pulse generator connected to a delay circuit, and the delay time between the laser pulse and the gate-on pulse was monitored with an oscilloscope. The gate-on duration or the PL observation period was adjusted from 50 ns to 4 μs so that clear PL spectra could be obtained.

III. RESULTS

The elemental compositions of all the $a-SiO_xN_y$:H and $a-SiN_z$:H films have been determined by XPS as shown in Table I. For $a-SiO_xN_y$:H films (samples A, B, and C), the nitrogen and the silicon contents decrease with a decrease in the gas flow ratio of SiH_4 to the sum of the other two gases [$SiH_4/(N_2O+N_2)$]. The silicon content decreases for $a-SiN_z$:H films (samples D, E, and F) with a similar decrease in the gas flow ratio of SiH_4 to the other two gases. If the apparent chemical composition of $a-SiO_xN_y$:H is expressed by the relation, $1/2x(SiO_2)+1/4y(Si_3N_4)$, the value $(1/2)x+(3/4)y$ becomes unity. The value becomes less than unity if silicon is present in surplus as compared to the above equation. Namely, the value can be regarded as an abundance ratio of atoms other than silicon to silicon atoms. For the sake of simplicity, the value is called the abundance ratio. The ratio approaches unity in the order from sample A to C, indicating that silicon is the most abundant in sample A and the least abundant in sample C. For $a-SiN_z$:H, the value $(3/4)z$ is the abundance ratio, which indicates that samples D and F are the most and the least abundant in silicon, respectively.

Figure 1 shows typical PL spectra in $a-SiO_xN_y$:H and $a-SiN_z$:H films observed at 10 K and their PLE spectra monitored at respective PL peak energies. A Gaussian-shaped broad PL band is observed in all the samples. The following three systematic trends can be observed as the abundance ratio increases regardless of whether the sample is $a-SiO_xN_y$:H or $a-SiN_z$:H.

(i) The PL spectrum shifts toward a higher energy.

(ii) It becomes broader.

(iii) The PLE threshold energy shifts toward a higher energy.

These trends are in agreement with the finding by other authors for $a-SiN_x$:H[16–18] and amorphous silicon carbide ($a-SiC_x$:H).[19,20] It is considered that the PLs shown in Fig. 1 are essentially identical and are due to radiative recombination within the localized states at the band tail.[10–15]

The objective of the present research is to elucidate various aspects of this band-tail PL. Appearance of similar PL has been often reported for various amorphous materials such as $a-SiN_x$:H, $a-SiC_x$:H, and amorphous silicon (a-Si:H).[16–23]

If the PL is related to band-tail states, the Urbach edge energy E_{edge} and the Urbach energy E_U can be estimated from the onset portion of the PLE spectrum. Generally, E_{edge} and E_U are defined by the following equation:[22]

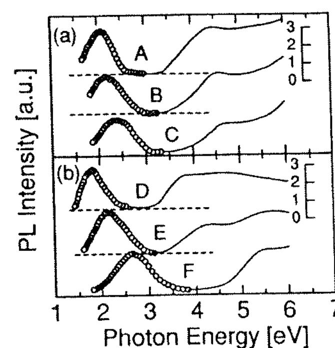

FIG. 1. PL (open circles) and PLE (solid lines) spectra in $a-SiO_xN_y$:H (a) and $a-SiN_z$:H (b) films observed at 10 K. Broken vertical lines indicate the detection limits.

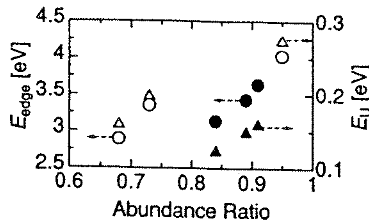

FIG. 2. The Urbach edge energy E_{edge} (circles) and the Urbach energy E_U (triangles) as a function of the abundance ratio. Closed and open symbols are for $a-SiO_xN_y$:H and $a-SiN_z$:H, respectively.

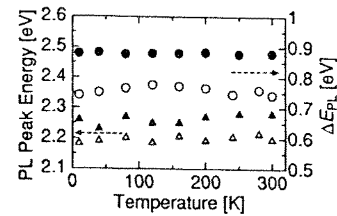

FIG. 4. Temperature dependence of the PL peak energy (triangles) and that of the PL FWHM ΔE_{PL} (circles) in the range of 10–300 K. Closed and open symbols are for samples B and E, respectively.

$$\alpha(h\nu)=\alpha_0 \exp[(h\nu-E_{edge})/E_U], \quad (1)$$

where α and $h\nu$ are the absorption coefficient and the photon energy, respectively. In PL excitation studies on $a-SiN_x$:H alloys by W. A. Jackson *et al.*[17] and on a-Si:H and its alloys by T. M. Searle and Jackson[21] the PLE spectrum was used instead of $\alpha(h\nu)$ on the assumption that the low-energy side of an excitation spectrum is proportional to α. Therefore, the PLE spectrum is also used instead of $\alpha(h\nu)$ in the present band-tail analysis. Figure 2 shows thus calculated E_{edge} and E_U. As the silicon abundance becomes less, E_{edge} and E_U increase monotonically in both cases of $a-SiO_xN_y$:H and $a-SiN_z$:H.

Figure 3 shows the normalized PL intensity as a function of the measurement temperature in the range of 10–300 K observed in samples B and E. The temperature dependence of the PL peak energy and that of the full width at half maximum (FWHM) of the PL band are shown in Fig. 4. The PL intensity decreases by an order of magnitude with an increase in the temperature, while the PL peak energy and the PL FWHM are almost independent. We have confirmed that almost the same dependence is observed in all the other samples.

To analyze the recombination processes of the photogenerated carriers, time-resolved PL measurements have been performed at room temperature. Figure 5 shows typical time-resolved PL spectra measured in samples B and F. Curve (i) is the spectrum obtained by measuring over the whole time region of 0.1 s without any delay. Curves (ii)–(vi) correspond to the spectra measured during given periods after the laser excitation. Furthermore, curve (i*) is the spectrum obtained by subtracting curve (ii) from curve (i). The PL peak energies were determined by fitting the PL spectra to Gaussian curves. A shift of the PL peak as a function of the delay time was observed, i.e., first to red, then to blue, and back to red again. Note that similar peak shifts were observed in all the samples.

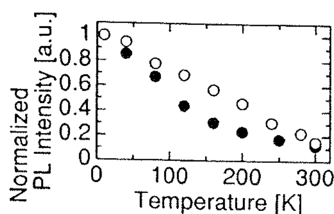

FIG. 3. Temperature dependence of the normalized PL intensity in the range of 10–300 K. Closed and open circles are for samples B and E, respectively.

Figure 6 shows the details of the shift as a function of time after excitation. The ordinate is the difference in the peak energy between each spectrum and the spectrum measured from 25 to 75 ns, e.g., curve (ii) in Fig. 5. The horizontal bar at each data point corresponds to the gate-on duration or the time interval used for the spectrum measurement. In all the samples, the PL peak energy shifts to a lower energy in the time regions from $\sim 10^{-8}$ to $\sim 2\times 10^{-7}$ s and from $\sim 7\times 10^{-6}$ to $\sim 10^{-4}$ s, while it shifts to a higher energy in the middle region from $\sim 2\times 10^{-7}$ to $\sim 7\times 10^{-6}$ s. The latter blueshift is more clearly seen in sample B than in A and in sample F than in E.

The height of the time-resolved PL spectrum was divided by the gate-on duration, and is shown as a function of the delay time in Fig. 7(a). The PL decays are nonexponential, ranging from $\sim 10^{-8}$ to 10^{-4} s, which indicates that the PL has a broad lifetime distribution. Hence, it is convenient to analyze the PL decay by assuming a distribution function $G(\tau)$ of lifetime τ. The function $G(\tau)$ is expressed by the equation,

$$G(\tau)=\text{const.} I(d \ln I/d \ln \tau), \quad (2)$$

where I is the PL intensity and τ is the lifetime. Figure 7(b) shows the product $\tau G(\tau)$ drawn by choosing $G(\tau)$ so as to yield the best fits to the decays according to the procedure suggested by Tsang and Street.[23] The lifetime distribution

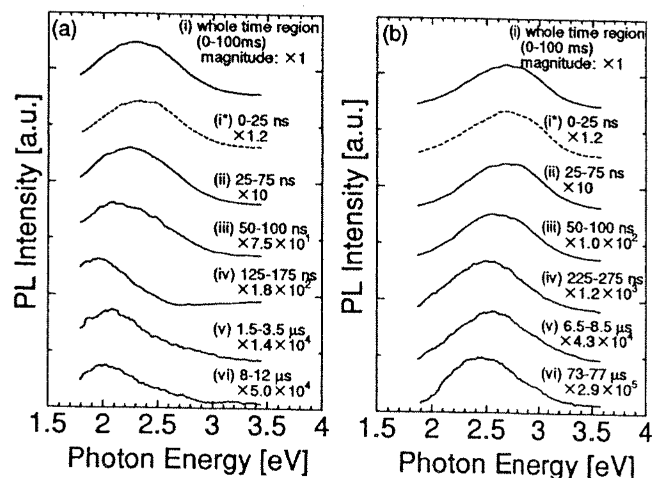

FIG. 5. Typical time-resolved PL spectra excited by 5.0-eV photons, observed in samples B (a) and F (b). Numerals following (i)–(vi) indicate given observation periods.

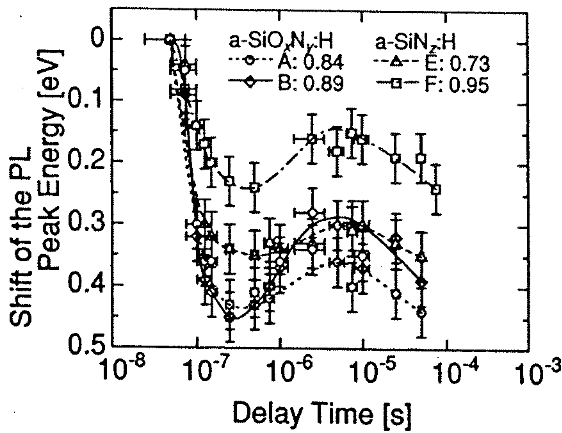

FIG. 6. Shift of the PL peak energy as a function of the time after excitation. Numerals next to the sample names are their abundance ratios.

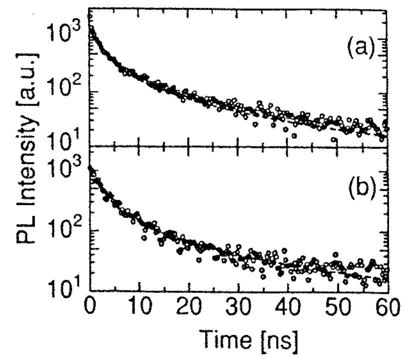

FIG. 8. Nanosecond-order decay at 10 K monitored at each PL peak in samples B (a) and E (b). Excitation was done by photons with an energy of 5.0 eV.

$\tau G(\tau)$ has a component that stretches over a wide range from 10^{-6} to 10^{-4} s besides a steeply dropping component around 10^{-7} s.

In Fig. 7(b), a steep drop in $\tau G(\tau)$ is seen at $\sim 10^{-7}$ s, the same time range wherein the initial redshift in the time-resolved spectra is observed. In order to study this further, the PL decay at this early stage was investigated using SR. Figure 8 shows typical nanosecond-order decay curves of PL in samples B and E excited by SR photons with an energy of 5.0 eV at 10 K. The decay curves monitored at respective PL emission peaks are nonexponential and can be expressed by a stretched exponential function,

$$I'(t) \propto (\beta/\tau')(\tau'/t)^{1-\beta} \exp[-(t/\tau')^{\beta}], \tag{3}$$

where I' is the PL intensity, t the time, τ' the effective lifetime, and β a parameter that has a value between 0 and 1. The curves in Fig. 8 are the results of the least-squares fit of the decay profiles to Eq. (3). The data satisfy Eq. (3) well, which is consistent with many reports indicating that the PL decay is described by the above equation for many amorphous materials.[10,14,18,24–28] The lifetime τ' is calculated to be 8.3 ns for sample B and 14.5 ns for sample E, while β is 0.4 for the two samples.

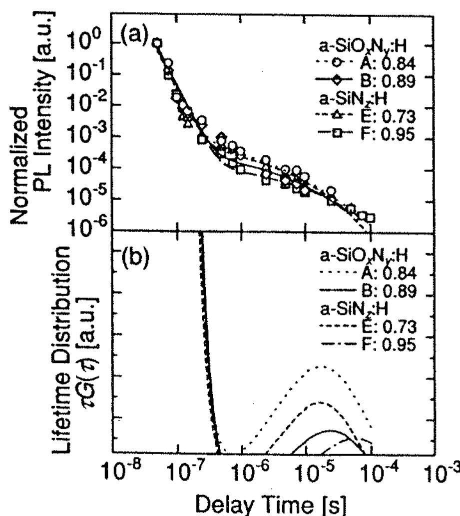

FIG. 7. PL decays (a) and PL lifetime distribution (b) measured in a-SiO_xN_y:H and a-SiN_z:H films, excited by 5.0-eV photons at room temperature. The lifetime distribution stretches over a time range from 10^{-8} to 10^{-4} s. Numerals next to the sample names are their abundance ratios.

The time at which $\tau G(\tau)$ shows the peak in Fig. 7(b) changes as a function of the abundance ration as shown by the circles in Fig. 9. Note that the PL intensity observed in sample D was too weak for this analysis. The changes in the effective lifetime τ' calculated for all the samples are also shown in Fig. 9 by the triangles. Both the two quantities become longer with an increase in the abundance ratio for both a-SiO_xN_y:H and a-SiN_z:H.

IV. DISCUSSION

Appearance of band-tail PL has been reported in many amorphous materials.[16–23] Following explanations are accepted to understand typical features of the band-tail PLs in a-SiN_x:H[16–18] and a-SiC_x:H.[19,20] As the nitrogen or carbon content increases, the band-gap energy increases, which leads to a blueshift of E_{edge}. This shifts the PL peak to a higher energy. In addition, nitrogen or carbon alloying induces the structural disorder, resulting in an increase in the width of the localized states denoted by E_U. This broadens the FWHM of the PL band. These phenomena have been called "antiparallel band-edge fluctuations," which is long-range disorder associated with spatial fluctuation of the elemental composition.[17,18,20,21]

As shown in Figs. 1 and 2, the PL peak energy and values of E_{edge} and E_U increase monotonically as the abundance ratio or the nitrogen content increases in the present a-SiN_z:H films. This confirms that the PL in the present a-SiN_z:H films is due to the band-tail recombination. Simi-

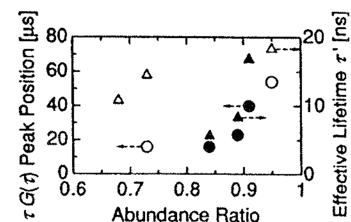

FIG. 9. The time at which $\tau G(\tau)$ shows the peak (circles) and the effective lifetime τ' (triangles) as a function of the abundance ratio. Closed and open symbols are for a-SiO_xN_y:H and a-SiN_z:H, respectively.

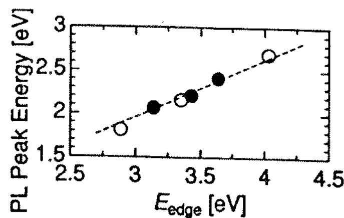

FIG. 10. Correlation between the Urbach edge energy E_{edge} and the PL peak energy. Closed and open circles are for $a-SiO_xN_y$:H and $a-SiN_z$:H, respectively.

lar shifts were also observed in $a-SiO_xN_y$:H films. Figure 10 shows the relation between E_{edge} and the PL peak energy, where a striking similarity between the two materials is illustrated. This similarity strongly indicates that the PLs observed in the present two kinds of samples are due to the same mechanism (=band-tail recombination) at the same chromophore. Using silicon oxynitride films prepared by rapid thermal nitridation of silicon dioxide in a hydrogen-free NO ambience, we have already clarified that the chromophore is the Si–N bond and has no relation to hydrogen.[11] In this case, it could be considered that $a-SiN_z$:H with a lot more Si–N bonds than in $a-SiO_xN_y$:H should give a stronger PL. However, this is not always the case in our results. The PL intensity is a function of the number of luminescence centers, the radiative recombination probability, and the nonradiative recombination probability. Since different materials would have different probabilities, the PL intensity is not always in proportion to the number of Si–N bonds.

The bandwidth of PL induced by the band-tail recombination should depend positively on the width of the localized states,[16–21] although the mechanism that determines the PL bandwidth is still to be discussed in amorphous materials. While the Stokes-shift model attributes the PL bandwidth to a strong electron-phonon coupling,[22,29,30] the static disorder or zero-phonon model assigns it to the distribution of carriers in either band tail resulting from structural disorder.[17,18,20,21] Since the two mechanisms can coexist, the FWHM of the PL band, ΔE_{PL}, is given by[18,20–22]

$$(\Delta E_{PL})^2=(\xi E_U)^2+(\Delta E_{e\text{-}ph})^2, \tag{4}$$

where ξ is a coefficient, E_U the Urbach energy, and $\Delta E_{e\text{-}ph}$ the increment in FWHM associated with the Stokes shift. Figure 11 shows the relation between E_U and ΔE_{PL}, indicating that ΔE_{PL} is proportional to E_U in each material. That each straight line passes the origin of the coordinate axes indicates that the effect of E_U, or that of structural disorder

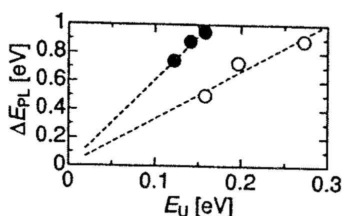

FIG. 11. Relation between the Urbach energy E_U and the FWHM of the PL spectrum ΔE_{PL}. Closed and open circles are for $a-SiO_xN_y$:H and $a-SiN_z$:H, respectively.

is more predominant than that of the electron-phonon coupling. Moreover, it has been known that E_U is composed of thermal disorder due to thermally induced network vibration and static disorder due to pure structural randomness.[22] If E_U is mainly due to the thermal disorder, the PL FWHM should depend on the temperature. However, it is almost constant in the range of 10–300 K as shown in Fig. 4, indicating that the effect of the static disorder is dominant in both materials.

Next, we discuss how the photogenerated carriers recombine via such localized band-tail states. As shown in Figs. 5 and 6, the PL peak shifts depending on the delay time, first to red, then to blue, and back to red again. Moreover, the broad distribution of PL lifetime, ranging from $\sim 10^{-8}$ to 10^{-4} s, is seen. This is another piece of evidence supporting the view that the PL is due to the band-tail recombination in the present two materials.[14,19,31–33] It is assumed that three different effects, namely, thermalization, Coulombic interaction, and distribution of localized states, influence the recombination process. The photogenerated carriers lose their energy by thermalization at the band-tail states, which induces the first redshift.[14,32,33] Assuming a tunneling process in the recombination, the PL lifetime becomes longer because the recombination probability decreases if the distance between the electron-hole pair is longer, while the Coulombic energy loss decreases. Hence, the PL shifts to a higher energy as the delay time increases.[14,19,32,33] The blueshift is more evident in sample B than in A and in sample F than in E. Namely, it is clearer in samples with lower permittivities (see the refractive indices listed in Table I). This indicates that the blueshift results from the Coulombic interaction. The final redshift is attributable to the extent of localization of carriers. Electrons and holes in the deeper states are more localized, which leads to a longer lifetime of the electron-hole pair in the frame of the radiative tunneling model.[14,19,32,33]

As shown in Fig. 7(b), the PL has two decay components. The fast decay component is known to be commonly observed in $a-SiC_x$:H[19] and $a-SiN_x$:H[18,28] but is absent in a-Si:H. This means that excitonlike recombination of electron-hole pairs is the radiative mechanism for the fast component, since strong Coulombic force due to the presence of carbon or nitrogen atoms accelerates the radiative recombination rate.[14,31] The electron-hole pairs that survived the excitonlike recombination are then thermalized into localized states. It is considered that recombination through radiative tunneling of these electron-hole pairs is responsible for the slow decay component, as in the case of similar PL decays reported in a-Si:H,[22,32] amorphous silicon oxide ($a-SiO_x$:H),[33] $a-SiC_x$:H,[19,31] and $a-SiN_x$:H.[14]

Finally, focusing on the width of the localized band-tail states, the structural inhomogeneity is compared between $a-SiO_xN_y$:H and $a-SiN_z$:H. The slopes of the straight lines shown in Fig. 11 are ~6.1 and ~3.4 for $a-SiO_xN_y$:H and $a-SiN_z$:H, respectively. It might be considered that these values should be similar in the two materials, since the PL origins are identical. The reason for this is that $a-SiO_xN_y$:H has a narrower band tail than $a-SiN_z$:H as is clearly indicated in Fig. 2 by its smaller values of E_U. On the other hand, if we compare PL lifetimes between the two

materials with the same abundance ratio, the lifetime is shorter in $a-SiO_xN_y:H$ than in $a-SiN_z:H$ as shown in Fig. 9. In the case of the band-tail recombination, a broader band tail brings a longer lifetime, since the photogenerated carriers can be thermalized into deeper localized states. All these results indicate that the degree of the structural disorder is smaller in $a-SiO_xN_y:H$ than in $a-SiN_z:H$. It is natural to consider that Si–O bonds are more flexible than Si–N bonds, since oxygen takes twofold coordination, whereas nitrogen takes threefold coordination. Therefore, the Si–O bonds can relieve the internal stress, which makes the structural disorder in $a-SiO_xN_y:H$ smaller.

V. CONCLUSION

Characterization of the PLs observed in $a-SiO_xN_y:H$ and $a-SiN_z:H$ films is carried out by investigating the PL band shape and the recombination process of photogenerated carriers. The PLs in the two materials have many similarities, and are considered to be due to the recombination between localized band-tail states associated with Si–N bonds. Further analyses on the PL decay process indicate that the recombination consists of two processes, namely, an exciton-like recombination process and a radiative tunneling recombination process.

The PL peak energy becomes higher and the width of the PL spectrum becomes wider if the abundance ratio of (nitrogen+oxygen) or that of nitrogen increases. This is caused by the increase in the band-gap energy and the increase in the width of band-tail states induced by the presence of nitrogen and oxygen. The width of band-tail states or the degree of structural inhomogeneity is smaller in $a-SiO_xN_y:H$ than in $a-SiN_z:H$. It is considered that the presence of oxygen atoms relieves the internal stress.

ACKNOWLEDGMENTS

This work was partly done in the 2001 Joint Studies Program of UVSOR Facility, Institute for Molecular Science, Okazaki, Japan. It was supported by Grants-in-Aid from the Japan Society for the Promotion of Science (JSPS) for JSPS Fellows (No. 1205733), for Scientific Research (B) (No. 12450132), and for Encouragement of Young Scientists (No. 12750307). A High-Tech Research Grant from the Ministry of Education, Culture, Sports, Science, and Technology of Japan is also appreciated.

[1] M. Murata, K. Yamauchi, H. Kojima, A. Yokoyama, T. Inoue, and T. Iwamori, J. Electrochem. Soc. **140**, 2346 (1993).
[2] P. Doshi, G. E. Jellison, Jr., and A. Rohatgi, Appl. Opt. **36**, 7826 (1997).
[3] H. Fukuda, T. Arakawa, and S. Ohno, Electron. Lett. **26**, 1505 (1990).
[4] M. Bhat, L. K. Han, D. Wristers, J. Yan, D. L. Kwong, and J. Fulford, Appl. Phys. Lett. **66**, 1225 (1995).
[5] K. B. Mogensen, P. Friis, J. Hubner, N. Petersen, A. M. Jorgensen, P. Telleman, and J. P. Kutter, Opt. Lett. **26**, 716 (2001).
[6] H. Kato, M. Fujimaki, T. Noma, and Y. Ohki, J. Appl. Phys. **91**, 6350 (2002).
[7] M. Modreanu, M. Gartner, and D. Cristea, Mater. Sci. Eng., C **19**, 225 (2002).
[8] M. J. Kerr, J. Schmidt, A. Cuevas, and J. H. Bultman, J. Appl. Phys. **89**, 3821 (2001).
[9] C. Boehme and G. Lucovsky, J. Appl. Phys. **88**, 6055 (2000).
[10] T. Noma, K. S. Seol, M. Fujimaki, H. Kato, T. Watanabe, and Y. Ohki, Jpn. J. Appl. Phys., Part 1 **39**, 6587 (2000).
[11] T. Noma, K. S. Seol, H. Kato, M. Fujimaki, and Y. Ohki, Appl. Phys. Lett. **79**, 1995 (2001).
[12] H. Kato, A. Masuzawa, T. Noma, K. S. Seol, and Y. Ohki, J. Phys.: Condens. Matter **13**, 6541 (2001).
[13] H. Kato, A. Masuzawa, H. Sato, T. Noma, K. S. Seol, M. Fujimaki, and Y. Ohki, J. Appl. Phys. **90**, 2216 (2001).
[14] K. S. Seol, T. Watanabe, M. Fujimaki, H. Kato, Y. Ohki, and M. Takiyama, Phys. Rev. B **62**, 1532 (2000).
[15] K. S. Seol, T. Futami, T. Watanabe, Y. Ohki, and M. Takiyama, J. Appl. Phys. **85**, 6746 (1999).
[16] I. G. Austin, W. A. Jackson, T. M. Searle, P. K. Bhat, and R. A. Gibson, Philos. Mag. B **52**, 271 (1985).
[17] W. A. Jackson, T. M. Searle, I. G. Austin, and R. A. Gibson, J. Non-Cryst. Solids **77&78**, 909 (1985).
[18] F. Giorgis, C. Vinegoni, and L. Pavesi, Phys. Rev. B **61**, 4693 (2000).
[19] W. Siebert, R. Carius, W. Fuhs, and K. Jahn, Phys. Status Solidi B **140**, 311 (1987).
[20] L. R. Tessler and I. Solomon, Phys. Rev. B **52**, 10 962 (1995).
[21] T. M. Searle and W. A. Jackson, Philos. Mag. B **60**, 237 (1989).
[22] R. A. Street, *Hydrogenated Amorphous Silicon* (Cambridge University Press, Cambridge, 1991).
[23] C. Tsang and R. A. Street, Phys. Rev. B **19**, 3027 (1979).
[24] G. Williams and D. C. Watts, Trans. Faraday Soc. **66**, 80 (1970).
[25] K. Murayama and T. Ninomiya, Solid State Commun. **53**, 125 (1985).
[26] N. Ookubo, H. Ono, Y. Ochiai, Y. Mochizuki, and S. Matsui, Appl. Phys. Lett. **61**, 940 (1992).
[27] K. Suzuki, G. Bley, U. Neukirch, J. Gutowski, N. Takojima, T. Sawada, and K. Imai, Solid State Commun. **105**, 571 (1998).
[28] F. Giorgis, C. F. Pirri, C. Vinegoni, and L. Pavesi, Phys. Rev. B **60**, 11 572 (1999).
[29] R. A. Street, Adv. Phys. **30**, 593 (1981).
[30] F. Boulitrop and D. J. Dunstan, Phys. Rev. B **28**, 5923 (1983).
[31] L. R. Tessler, Solid State Commun. **111**, 193 (1999).
[32] B. A. Wilson and T. P. Kerwin, Phys. Rev. B **25**, 5276 (1982).
[33] R. A. Street, Solid State Commun. **34**, 157 (1980).